NOTICE

AVIS

The quality of this microform is heavily dependent upon the quality of the original thesis submitted for microfilming. Every effort has been made to ensure the highest quality of reproduction possible.

If pages are missing, contact the university which granted the degree.

Some pages may have indistinct print especially if the original pages were typed with a poor typewriter ribbon or if the university sent us an inferior photocopy.

Previously copyrighted materials (journal articles, published tests, etc.) are not filmed.

Reproduction in full or in part of this microform is governed by the Canadian Copyright Act, R.S.C. 1970, c. C-30.

La qualité de cette microforme dépend grandement de la qualité de la thèse soumise au microfilmage. Nous avons tout fait pour assurer une qualité supérieure de reproduction.

S'il manque des pages, veuillez communiquer avec l'université qui a conféré le grade.

La qualité d'impression de certaines pages peut laisser à désirer, surtout si les pages originales ont été dactylographiées à l'aide d'un ruban usé ou si l'université nous a fait parvenir une photocopie de qualité inférieure.

Les documents qui font déjà l'objet d'un droit d'auteur (articles de revue, tests publiés, etc.) ne sont pas microfilmés.

La reproduction, même partielle, de cette microforme est soumise à la Loi canadienne sur le droit d'auteur, SRC 1970, c. C-30.

Canada

THE UNIVERSITY OF ALBERTA

ULTRAHIGH SPECTRAL BRIGHTNESS KRYPTON FLUORIDE LASER SOURCE

BY

Xinxin Shan

A THESIS

SUBMITTED TO THE FACULTY OF GRADUATE STUDIES AND RESEARCH

IN PARTIAL FULFILMENT OF THE REQUIREMENTS FOR THE DEGREE

OF Master of Science

Department Of Electrical Engineering

EDMONTON, ALBERTA

FALL, 1988

THE UNIVERSITY OF ALBERTA

RELEASE FORM

NAME OF AUTHOR: Xinxin Shan

TITIE OF THSIS: Ultrahigh Spectral Brightness
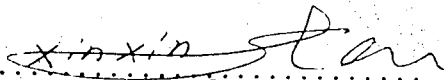Krypton Fluoride Laser Source

DEGREE: Master of Science

YEAR THIS DEGREE GRANTED: Fall, 1988

Permission is hereby granted to THE UNIVERSITY OF ALBERTA LIBRARY to reproduce single copies of this thesis and to lend or sell such copies for private, scholarly or scientific research purpose only.

The author reserves other publication rights, and neither the thesis nor extensive extracts from it may be printed or otherwise reproduced without the author's written permission.

Date: Aug 24, 1988

....
(Student's signature)

....

....

....
(Student's permanent address)

THE UNIVERSITY OF ALBERTA

FACULTY OF GRADUATE STUDIES AND RESEARCH

The undersigned certify that they have read, and
recommend to the Faculty of Graduate Studies and Research
for acceptance, a thesis entitled Ultrahigh Spectral
Brightness Krypton Fluoride Laser Source submitted by
Xinxin Shan in partial fulfilment of the requirements for
the degree of Master of Science.

....
(Supervisor)

....
(Supervisor)

....

....

Date:..........................

ABSTRACT

A number of excimer laser applications require ultrahigh spectral purity sources approaching transform limited linewidth. The research for this thesis was directed at improving the spectral quality of an existing KrF laser system. The project involved studying and implementing an ultrahigh spectral brightness KrF laser system. A narrow linewidth, ~ 100MHz, has been obtained by injection locking the KrF laser system using the amplified, frequency doubled, output of a CW argon ion laser.

Measurements of the variation in small signal gain and saturation have been made in the peak gain region of 248.2 to 248.4nm for a KrF laser operating at 1.7atm, pressure. Injection of an unstable resonator KrF laser was characterized as a function of input power using the argon ion laser seed pulse source. The output injection fraction was found to range from 3.4% to 93% over an input injection power range of 0.075 W to 5.8 KW.

ACKNOWLEDGEMENTS

TABLE OF CONTENTS

LIST OF TABLES

LIST OF FIGURES

CHAPTER 1

INTRODUCTION

Excimer lasers are now being employed in numerous applications which require reliable narrow linewidth output spectral characteristics. These include lithography of microelectronic circuits and laser fusion studies in which nonlinear optical pulse compression techniques are employed.

For applications in electronic circuit lithography, ultraviolet (UV) wavelength lasers allow the fabrication of submicron feature sizes and thus very high device density for VLSI circuits. Large field of view, diffraction limited optical imaging is required to project the required patterns onto the silicon wafers. Optical materials become very dispersive in the ultraviolet wavelength region which makes it difficult to design optical systems that remain diffraction limited over broad wavelength regions. Even the bandwidth of a normal KrF laser system, 1.5THz, is large enough to require very complex lenses in such systems and thus linewidth narrowing is probably required. The required linewidth, ~ 30GHz [1], is not in itself very difficult to obtain. However, it is necessary to have very high reliability and very good reproducibility of operating characteristics.

Ultraviolet wavelength laser are also good candidates for laser fusion drivers because of the very efficient absorption of the short

1

wavelength laser radiation by the plasma and the resultant high hydrodynamic efficiency of the UV laser-produced ablation. Rare gas halide excimer lasers have been identified as potentially efficient sources of high-power UV radiation [2,3]. The most popular candidate is the krypton fluoride (KrF) laser, principally because of the fact that it has a high predicted efficiency, on the order of 10%, and its wavelenghth, 248nm, is far into the UV wavelength range.

The desirable properties of the KrF laser include: (1) it has a gas laser medium, capable of sustaining high repetition rates without damage to the medium; (2) the operating pressure is relatively low, 1-2 atm., minimizing many practical difficulties of operating large aperture amplifiers; (3) KrF can be efficiently pumped by high - voltage, large - area electron beams at high current densities for pulse lengths on the order a microsecond; (4) KrF lasers presently have achieved an overall efficiency of 4 - 7% approaching the value required for an Inertial Confinement Fusion (ICF) reactor driver; (5) the wavelength is still long enough that high damage threshold, > 5 J/cm^2, optical materials are still available for the fabrication of optical components.

Because of these desirable properties a KrF laser system has been developed in our laboratory over the last 8 years in order to carry out laser fusion related studies. This system consists of four discharge laser modules, an electron beam pumped amplifier module, a nonlinear optical pulse compression system and an evacuated target chamber

facility. The front end of this laser system is line-narrowed, using injection locking from an etalon tuned master oscillator.

One, of the disadvantages of KrF lasers is the long pulse length which is not well suited for nanosecond duration high intensity experiments. Therefore, the development of very high power short pulse lasers in this wavelength, region requires the application of optical pulse compression techniques. For many present and proposed applications optical pulse compression techniques such as stimulated Raman and Brillouin scattering may be required [2-6]. For these processes, a high degree of monochromaticity is required, on the order of the natural linewidth of the scattering process. The Raman backscatter compression technique in high pressure methane gas which was originally used in our laboratory only required a linewidth of ~ 3 GHz. Recently, however, the generation of subnanosecond KrF laser pulses by stimulated Brillouin scattering (SBS), has been demonstrated in high pressure gases [6]. However, for efficient SBS pulse compression, even narrower linewidths, of the order of 100 MHz and less, are required [4,5,6].

Previous studies [2,7,9] have shown that substantial improvement in beam spectral and spatial quality is obtained by using the output of a narrow bandwidth, stable resonator, master oscillator to injection lock a high-energy, unstable resonator slave oscillator. The linewidth generated from such an etalon-narrowed, injection-locked oscillator-amplifier KrF laser system is ~ 3GHz [2,7]. This was the

technique originally used to generate the narrow linewidth required for the Raman backscatter pulse compression process in methane gas. In order to improve the operating characteristics of our KrF laser system to meet the need of SBS pulse compression a new technique was developed to obtain ultrahigh spectral brightness KrF excimer laser radiation with a spectral width of ~ 100 MHz. This technique involves pulsed dye laser amplification of the 5 MHz linewidth, CW radiation from an argon ion laser at 496.5 nm. The resultant output pulse is frequency doubled in a nonlinear crystal and this radiation is used to injection lock a KrF laser module.

This new technique of using an argon ion seed laser has been developed and investigated in this thesis. The initial experimental measurements involved the study of small signal gain and saturation in the peak gain region of 248.2 to 248.4 nm for a KrF laser operating at 1.7 atm pressure. This was done to determine how well matched the argon ion wavelength is to the KrF laser spectral gain profile. As part of this work a pulsed dye laser amplifier system was designed and optimized for the production of the seed pulses. Thereafter, the injection locking of the KrF laser was studied as a function of input power in order to assess the minimum input power required to obtain reliable operation.

In Chapter 2, the background and theory of narrow bandwidth KrF laser sources is briefly reviewed. In Chapter 3, the experimental arrangements are described in detail including the argon ion laser, dye

laser, UV frequency conversion, injection locking system and diagnostic systems. In Chapter 4, the main experimental results are given, analyzed and discussed. The conclusion of this thesis is given in Chapter 5 together with some suggestions for future work.

CHAPTER 2

BACKGROUND AND THEORY

One of the reasons for the high efficiency of rare gas halide (RGH) excimer lasers is the presence of a dissociative ground state so that it is impossible to have quenching of the population inversion. This can be seen if one looks at the energy level diagram as a function of interatomic spacing, as shown in Fig. 1.

The KrF laser transitions are identified as the $B^2\Sigma \longrightarrow X^2\Sigma$ transitions of RGH excimer molecules, comprised of one rare gas atom and one halogen atom [11,12]. The excited upper state has a substantial potential well which traps the excited pair of atoms. From the upper state the molecule can undergo either a collisional or radiative transition with a lifetime of a few nanoseconds. The ground state of the transition is strictly repulsive except for the Xenon halides which do possess a shallow potential well on the order of 0.04 eV [12]. KrF is the prefered candidate for high energy laser systems since it has been found that the intrinsic efficiency of the KrF laser is greatest of the excimer lasers. The dominant KrF formation reaction is:

$$Kr^* + F_2 \longrightarrow KrF^* + F$$
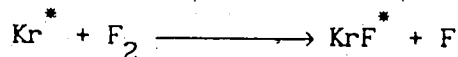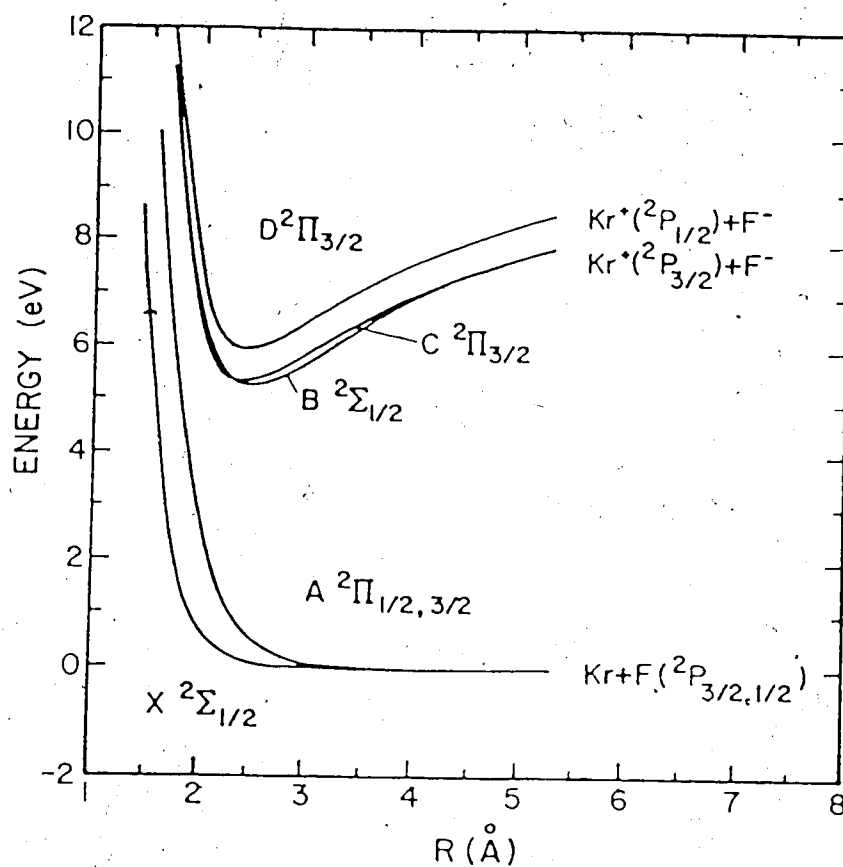
Fig.1 Energy levels of the KrF molecule as a function of interatomic separation, R.

This process is very rapid, occuring in a time typically of the order of 10ns and is very efficient in producing excited rare gas halide products [12]. However, the detailed kinetics of the excited states species in a KrF laser are very complex involving over 10 rate equations [12] and can only be modelled using numerical simulation techniques.

While excimer lasers can be efficient, their upper state lifetimes are very short, so they cannot store their energy in a population inversion such as other laser systems (e.g. CO_2 or Nd:Glass). Efficient operation requires continuous extraction in order to utilise the energy delivered by the electrical excitation. Typical electrical pump durations are 10-5000 ns. The most efficient systems are typically those with the longer pulse duration.

For many applications, such as laser fusion, short pulses on the order of a nanosecond are required and thus additional techniques of pulse compression are necessary. One of these techniques [4,5,6], stimulated Brillouin scattering (SBS), has been demonstrated for the generation and amplification of nanosecond and subnanosecond duration ultraviolet laser pulses. In this technique the stored energy can be continuously extracted from the KrF laser module for the duration of the laser excitation and the resultant long KrF pulse can then be used to pump an SBS conversion cell. This process is illustrated in Fig.2(a) and 2(b). When a long pump laser pulse propagates through a gaseous medium containing sulfur hexafluoride (SF_6) gas, the pump light with
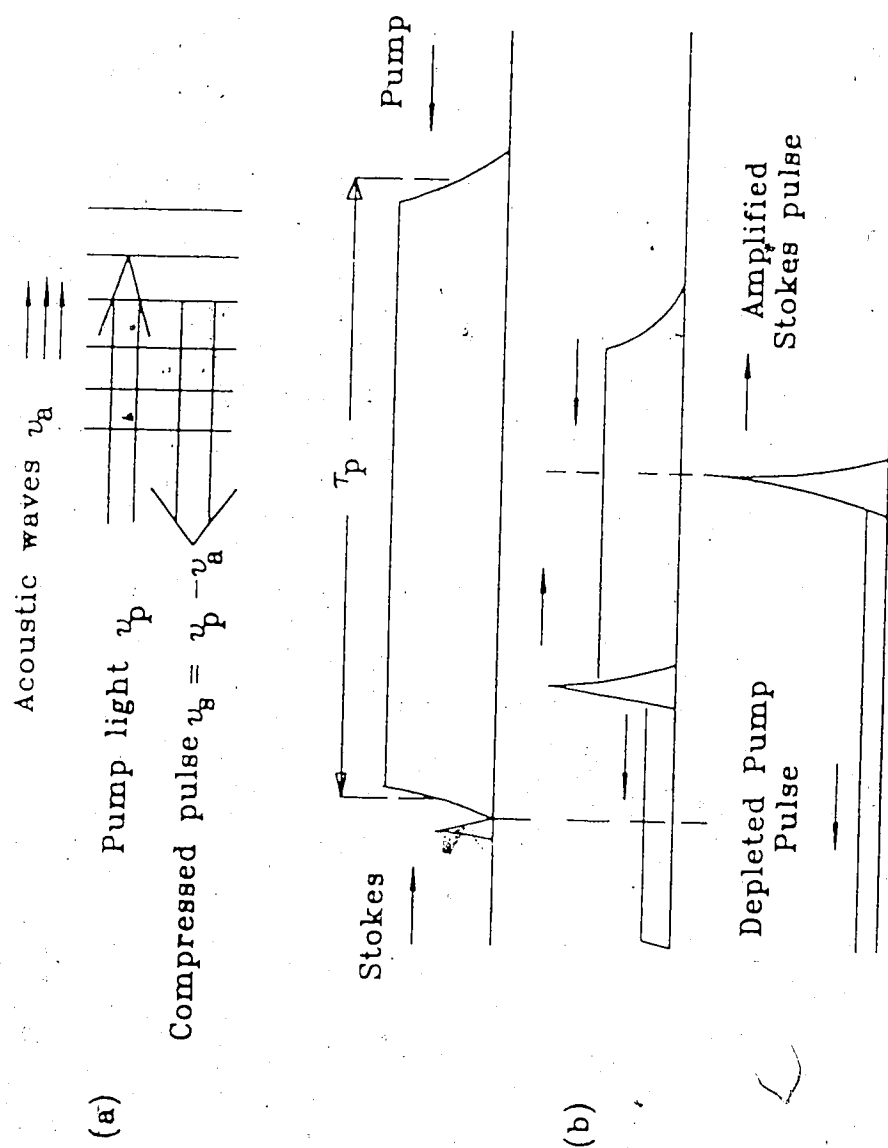
Fig.2 (a). Schematic diagram illustrating backward Brillouin
scattering pulse compression process.
(b). Schmatical representation, of the optical
pulse compression technique.

frequency υ_p can interact with an acoustic wave at frequency υ_a in the gas leading to scattered light at the Stokes shifted frequency of $\upsilon_s = \upsilon_p - \upsilon_a$. High efficiency is achieved by injecting a short pulse at frequency υ_s into the cell in the opposite direction to the pump pulse as it reaches the exit window. The energy from the long pulse is converted into the Stokes shifted pulse through the Brillouin 3-wave interaction process in the medium..

The best results to date, using a laser linewidth on the order of 1 GHz, shows compression to an average pulse duration of 390 ps with extraction efficiencies of 40 percent [6]. However, the experimental results [5,6] clearly show that to obtain maximum efficiency for this process, laser linewidths approaching the natural linewidth of the SBS mode, $\Delta\upsilon \sim 100$ MHz, are required. If such linewidths could be obtained, conversion efficiencies approaching 80% may be possible. The original oscillator in the KrF laser front end system had a linewidth of 3 GHz which was subsequently narrowed to 1 GHz. However, this is still too large to achieve the maximum efficiency from the SBS pulse compression system. Thus a new system to generate higher spectral purity radiation was required.

There are a number of techniques which have been used in the past to generate narrow linewidth KrF laser radiation. These include intracavity prism tuning [13], grating tuning at grazing incidence [14], etalon tuning [2,7] and injection locking using frequency doubled dye laser radiation [15] with output linewidths of $\sim$ 100GHz, $\sim$ 10GHz,

~ 3GHz and ~ 150 MHz respectively.

Motivated by the requirement of ultra-narrow linewidth for the SBS pulse compression system a much narrower linewidth front-end laser source was proposed and developed for this thesis project. The KrF laser amplifier was modified by externally narrowing the radiation linewidth. The start of the new UV source is an argon laser operating at 496.5 nm. The very narrow bandwidth is achieved by the combination of a prism and an etalon in the argon laser cavity. The initial radiation is then amplified in a three stage dye amplifier system and frequency doubled. Finally, the radiation is used to injection lock an unstable resonator KrF laser module. The layout is shown in block diagram form in Fig. 3.

The injection-locked amplifier is a high Fresnel number unstable resonator which can be analyzed using geometrical optics following the approach of Siegman [16]. The use of an unstable resonator combines the advantages of large mode volume with low-order mode operation, yielding a near diffraction-limited beam [16]. The positive-branch confocal resonator is particularly useful in that it can give a collimated output beam and has no internal focal points. However, unstable resonators do not lend themselves readily to conventional tuning and line-narrowing techniques. These methods can greatly complicate the otherwise simple cavity and, again, place limitations on peak pulse powers. Thus, different techniques are required. By using injection mode locking one can force the laser to run at the wavelength and
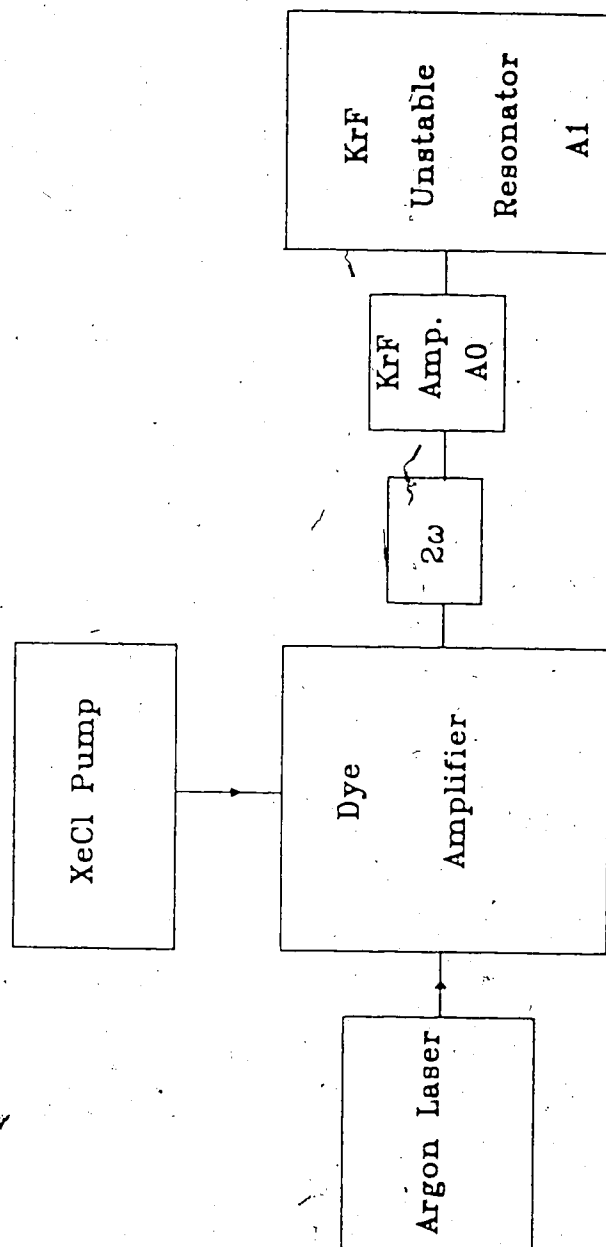
Fig. 3 The layout of the injection locked ultrahigh spectral brightness KrF laser source

bandwidth of a low power injected beam, while eliminating the need for any dispersive elements. The injection locking of unstable resonators was first described experimentally by BUCZEK, et al. [17], who used low power CO_2 lasers with a resulting power ratio, $P_{out}/P_{in} \sim 100$. We know that the injected power required to reliably lock is proportional to the number of transverse modes, m, which oscillate in the laser cavity[18]. Thus ,

$$P_{inj} \quad \propto \quad m \; = CF^2 \qquad\qquad (2.1)$$

where C is a constant and F is the Fresnel number of the cavity. Therefore, single-mode operation minimizes the required injection power in addition to minimizing beam divergence. The injection power required for complete locking will also depend on the difference between the free-running peak and locked wavelength, as well as on the pulse duration and total cavity losses.

The theoretical limits to linewidth and beam divergence of the unstable resonator output are given by the transform frequency spectrum of the output pulse shape and the diffraction of the finite output beam size. It can be easily shown by taking the Fourier transform of the time dependent electric field that any pulse of finite duration will have a finite spectral bandwidth. The minimum bandwidth, Δv, for a pulse of duration Δt is given by [19],

$$\Delta v \; = \; \frac{K}{\Delta t} \qquad\qquad (2.2)$$

where K is a constant of order unity which depends on the pulse shape. For Gaussian temporal and spectral shapes the constant $K = (2\ln2)/\pi = 0.441$. For a transform limited 20ns duration Gaussian pulse, the frequency bandwidth is 22 MHz.

The beam divergence can be calculated for a TEM_{00} mode Gaussian beam and is given by [20],

$$\theta_G = \frac{2\lambda}{\pi\omega_0} \qquad (2.3)$$

where θ_G is the full width divergence angle at the e^{-1} field amplitude points, ω_0 is the Gaussian beam waist and λ is the wavelength of the radiation. For a Gaussian beam with a beamwaist diameter of 2.5cm, at the full width half intensity points, $\omega_0 = 2.124$ cm and $\theta_G = 7.4$ μrad which gives a divergence angle of 4.4μrad at the half intensity points of the beam. For comparison, a coherent flat-top profile of radius r_0 produces a far field Airy function intensity pattern given by [21],

$$I(\theta) = I_0\left[\frac{J_1(2\pi r_0\theta/\lambda)}{(\pi r_0\theta/\lambda)}\right]^2 \qquad (2.4)$$

where I_0 is the peak intensity, J_1 is the first order Bessel function and θ is the angular position relative to the central beam axis. From this equation the full width half intensity divergence angle, θ_F, for a flat top initial beam profile of radius r_0 is given by

$$\theta_F = 0.514 \; \frac{\overline{\quad}}{r_0} \qquad\qquad\qquad (2.5)$$

For a 2.5cm diameter KrF laser beam this would give a divergence angle of 10.2 μrad the half intensity position. The actual output of .the unstable resonator module is something between the above two cases and thus for a 2.5cm output beam diameter we would expect a diffraction limited output beam divergence of between 4 and 10 μrad.

To date, the best linewidth generated from the etalon tuned KrF master oscillator in our laboratory is 2.5 GHz [7]. In order to achieve this, three etalons were employed within the stable resonator cavity. The elements are an air-spaced 0.1mm gap and solid 0.5mm and 3.0mm fused silica flats respectively with 75% reflectivity coatings. Fig. 4 shows the transmission of the three individual tuning etalons and the combined transmission of all three when properly tuned. The best linewidths obtained from the direct etalon tuned KrF oscillator source with optimum tuning is about 2.5 GHz. Additional line narrowing to $\Delta v \cong 1$ GHz has been achieved through the use of a 1 GHz bandpass external etalon at the output of the injection locked unstable resonator. This technique is quite cumbersome since temperature changes in the laboratory cause the spectral peaks of the master oscillator and external etalon to drift, necessitating frequent retuning of the system. In addition, there is a large optical loss in the external etalon element.
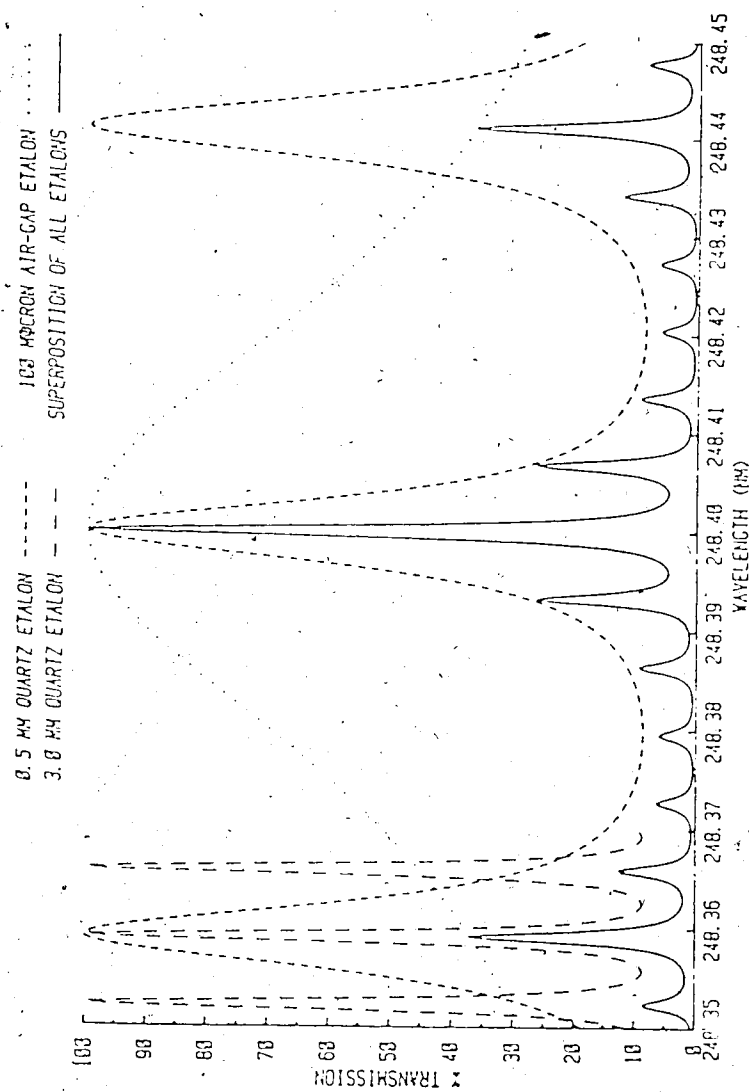
Fig.4 Transmission curves for the three individual tuning etalons
and the combination of three when properly tuned.

Using a frequency doubled tunable dye las source for injection locking it has been shown [15] that spectral widths of 150±30 MHZ can be obtained. In principle, even narrower linewidth, tunable, ultrahigh spectral brightness KrF excimer laser sources are possible using this technique. However, the operation and tuning of an ultra-narrow linewidth dye laser system to keep it matched exactly to the peak KrF wavelength requires a significant amount of maintenance and adjustment. In the present system the use of an argon ion laser both simplifies and increases the reliability of the system.

For the implementation of the proposed system two key issues had to be addressed. Firstly, the available literature [22-26] did not precisely indicate the peak wavelength for the KrF transition . Thus it was important to identity this peak wavelength and determine how accurately the frequency doubled argon ion laser wavelength would match this wavelength. The second question concerned the power requ. to achieve good injection locking, and thus the fractional output injection locking had to be determined as a function of input power.

In order to address the first key question for the proposed technique, measurements of small signal gain have been made in the peak gain region for a KrF laser module [27]. In order to carry out these experiments a dye amplifier system was required and part of the experimental project involved designing and optimizing such a system. Such dye amplifier systems have been developed previously and the starting point for the present design was taken from Hawkins et al

[15]. A 3 stage amplifier system using Coumarin 500 dye pumped with 16mJ of XeCl light produced an amplification of a 51mW input signal to 78KW of output power.

The results of the gain measurements indicated that the frequency doubled argon ion laser radiation at 248.25 nm falls within the peak gain region of the KrF laser.

The next key question involved the minimum input power required to achieve good injection locking. The second set of experiments were thus designed to characterize the output radiation of the KrF laser as a function of input power for input power levels of 0.075 W to 5800W which gave output injection locked fractions ranging from 3% to 92%.

EXPERIMENTAL SET UP

3.1. Main KrF laser system

The main KrF laser system, constructed for laser fusion related studies, consists of three major components. These are the UV laser front end, the discharge and electron beam pumped power amplifiers, and the Brillouin optical pulse compressor. The final beam is directed to a target chamber where the laser plasma interaction experiments are carried out. A schematic diagram of the front-end and Brillouin compressor systems is shown in Fig. 5. As discussed previously the master oscillator was equipped with a multi-etalon system to control the laser linewidth. As a result of this thesis work the master oscillator has now been replaced by an ultrahigh spectral brightness UV source as shown schematically in Fig 3. Following the oscillator stage, there are two other amplifiers A2, A3 which generate 1.0 J, 20ns duration pulses each. Part of the laser beam is also used to trigger and extract the e-beam amplifier module. The remaining part of the laser radiation is used to pump the system for pulse shortening by nonlinear optical techniques.

Fig. 6 and Table 1. give the principle characteristics of the unstable resonator slave oscillator. This unstable resonator configuration was used previously with the etalon tuned oscillator and throughout the present injection locking experiments.
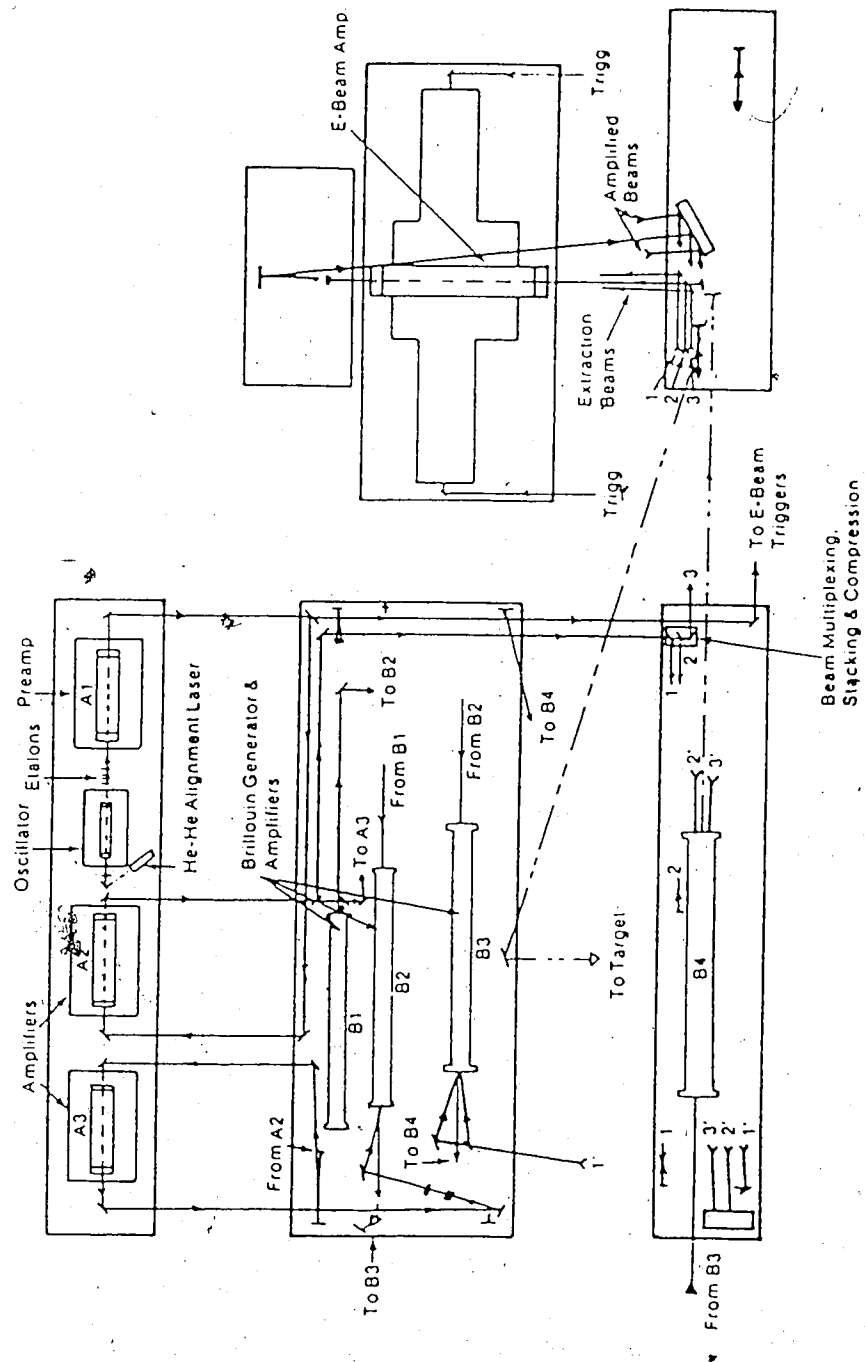
Fig. 5 The schematic diagram of the front end KrF and complete
       SBS compressor system.

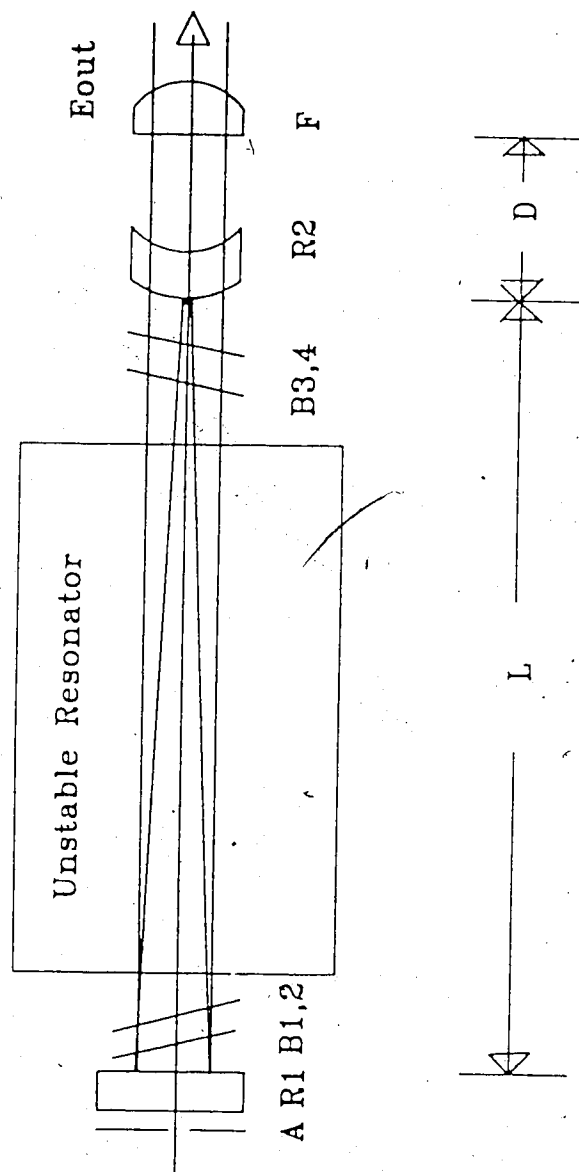
Fig.6 Schematic diagram of the unstable resonator.

Experimental layout: A-input aperture, B1-4 – Quartz
plates at Brewster's angle, F- collimating lens, R1 – 90%
flat mirror, R2 – 2mm diameter concave mirror.

Table I. Parameters of Unstable Resonator Module A1

Cavity length	1.6m
Reflection of flat mirror, R1	90%
Reflection of convex mirror, R2	100%
Diameter of convex mirror, R2	2mm
Radius of curvature of R2	0.6m
Distance to collimating lens, D	54cm
Focal length of collimating lens, F	4m
Output energy	400mJ
Duration of pulse	24ns
Output beam cross-section	24mm diameter
Gas mix - $He:Kr:F_2$	0.896:0.10:0.04
Total gas pressure	1.7atm.
Discharge volume	25x35x960mm
Discharge voltage	70Kv

3.2. Argon Ion Laser Based Front End System

For the present experiments a commercial, prism tuned, and etalon narrowed argon ion laser was employed. Two different lasers were used during the course of these experiments. These were a Spectra-Physics model 154 and a Coherent model 90-5. Both are nominally 5 W (all line) output power units. The former was used in most of the small signal gain and saturation measurements and the latter was used in the

22

measurements of injection mode locking. For the former the beam diameter of the laser is 1.25mm at the e^{-2} intensity points and the beam divergence is about 0.69 mrad. For the newer Coherent laser the beam diameter of the laser is 1.47mm at the e^{-2} intensity points and the beam divergence is about 0.44 mrad. Fig. 7 illustrates the longitudinal mode structure of the resonator with a tuning etalon which was similar for both lasers.

Initially, the Spectra Physics laser was operated without the extra tuning etalon giving a full natural linewidth of ~ 5 GHz for most of the small signal gain and saturation measurements. However, for a few of the measurements the tuning etalon was inserted to give a very narrow linewidth, ~ 3MHz, to verify that the gain was the same as obtained with the 5GHz linewidth source. Because of the rapid drop in output power as the laser tube aged in the Spectra Physics laser it was replaced with a newly purchased Coherent laser for subsequent experiments. The very narrow linewidth mode was subsequently used in all the injection mode locked measurements. The intracavity etalon for the Coherent laser was temperature stabilized for added stability and the manufacturer's specification for the linewidth in this case was less than 5MHz.

The argon ion and dye laser amplifier system is shown in Fig.8. The green, 496.5 nm, light was gated to give a pulse output of 200 ns duration, by means of an electro-optical pulse switch and a polarizer. The gating reduced the amount of scattered high intensity argon ion
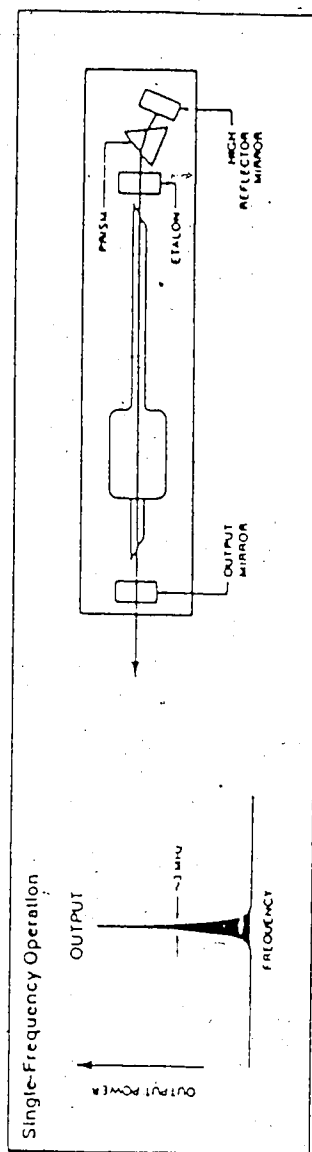
Fig. 7 Schematic diagram of the longitudinal mode structure and etalon line narrowed, frequency tuned, argon ion laser.
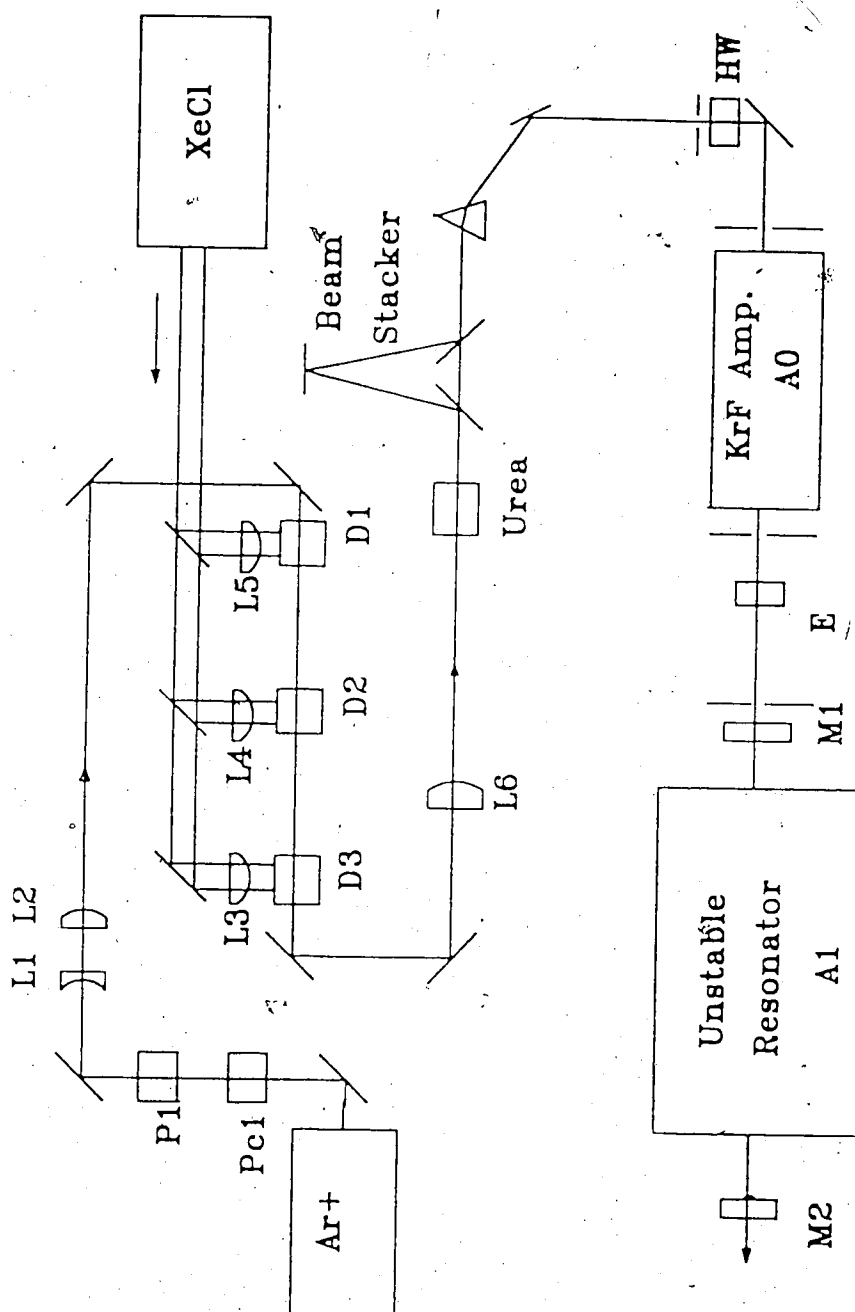
Fig. 8 The experimental arrangement of the argon ion laser and dye
amplifier system and KrF system.

Experimental layout: L1-L6 -Lenses, Ar$^+$-argon ion laser,
D1-D3- Coumarin dye cells, E - etalon, M1-90% reflective
mirror, M2 - meniscus mirror, Pc1- pockel's cell, P1 -
polarizor, Urea - frequency doubling crystal, A0-A1 -
discharge KrF laser modules, HW - half wave plate.

laser radiation in the laboratory, reduced the cw background signals on the detectors used in the experiment and reduced thermal heating and resulting optical distortion in the dye cells. The pulse gating system was not available for the initial experiments and was not used in the saturation and small gain measurements. The light was collimated into the three stage dye amplifier by a beam telescope which consisted of a negative 10cm lens followed by a positive 25cm lens as shown in Fig. 8. This lens system produced a beam waist of 178μm diameter located in the centre of the first stage dye cell.

This green light was subsequently amplified in the three stage dye amplifier system as shown in Fig. 8. The three dye cells were 10, 20 and 20 mm long respectively and were filled with solutions of Coumarin 500 dye dissolved in a mixture of 95% dioxane and 5% ethanol at a concentration of 1.25×10^{-2} M. The dye amplifier was pumped with a 17 mJ, 6.5 ns duration XeCl laser pulse split into three parts. For the initial gain and saturation measurements the beam was split using knife edge aluminized mirrors to intercept pieces of the beam. Subsequently, for the injection experiments the beam was split into three parts, 8%, 27% and 65% using an uncoated quartz beam splitter, a partial reflector mirror and an aluminium mirror respectively. The pump beams were focussed into the dye cells using cylindrical lenses of 75, 100 and 200 mm focal lengths respectively. The foci of the lenses were located at 0.25mm, 0.5mm and 0.75mm respectively inside the dye cell windows. For simplicity, non-flowing dye cells were used in the present system since a maximum repetition rate of 0.5Hz was anticipated. The dye cells were

tilted at an angle of ~ 15° to avoid lasing from the dye cell window reflections. Resultant output powers in excess of 70 KW were obtained in 5 ns pulses at the end of the dye amplifier chain. As shown in Fig. 8, the distance between the telescope lenses and the dye cell was more than 1 meter so that amplification of backscattered light from the lens faces could be avoided.

The green laser line at 496.5 nm was converted to 248.25 nm using type I frequency doubling in a urea crystal [28]. The crystal was 8 mm long and capable of giving a conversion efficiency of about $0.7 \times 10^{-4} W^{-1}$ for single transverse mode radiation at room temperature. The laser was focussed into the crystal using a 500 mm focal length lens. The distance between the lens and crystal was 42 cm and focal spot size just at the entrance of the crystal was ~ 300μm. The angle of incidence on the crystal was nearly zero degrees as the crystal was cut for 496 nm type I operation. Output powers in excess of 2.5 kW in a pulse of 3.5ns duration were obtained at the exit of the crystal when the argon ion laser input power exceeded 60m and the XeCl laser pump energy was 16mJ.

For the injection experiments, pulsed output powers of 2.5 kW were normally used since the argon ion laser input power was typically 51mW and the XeCl laser pump energy was 16mJ. The pulse duration, 3.5ns, was too short for achieving optimum injection so a pulse splitter/delay unit was employed to obtain longer pulses as shown in Fig. 8. The UV beam was split using a 50% mirror and half of the pulse was sent

through an optical delay system. The two beams were recombined using a second 50% beam splitter. The overall transmission of the system was ~43%. Alignment of the output beams to make them perfectly parallel required careful adjustment of the beam delay mirrors. We did not use the pulse splitter/delay system for the initial small signal gain measurements.

The UV beam was then passed through a prism to separate out the original green radiation and finally through an alignment pinhole and half wave plate to achieve the correct vertical polarization for the injection locking experiments. The vertically polarized light was then amplified in a single pass KrF amplifier module. This amplifier module, which was the old original master oscillator module had a 30cm gain length with a single pass small signal gain of 100.

3.3. Small Signal Gain Experiments

As shown in Fig.9, for the small signal gain versus wavelength experiments the tunable wavelength source was obtained by etalon tuning a KrF master oscillator module. The KrF laser oscillator and amplifier modules used in this experiment are the pulse charged, photo-preionized discharge modules of the type described previously. The master oscillator is a reduced size version of the amplifier modules with a gain length of 30 cm and a stable resonator optical cavity employing a concave 4 metre radius of curvature 100% reflective mirror and a flat 90% reflective output mirror. Transverse mode quality was controlled by means of a 2mm diameter aperture in the resonator cavity. For most of
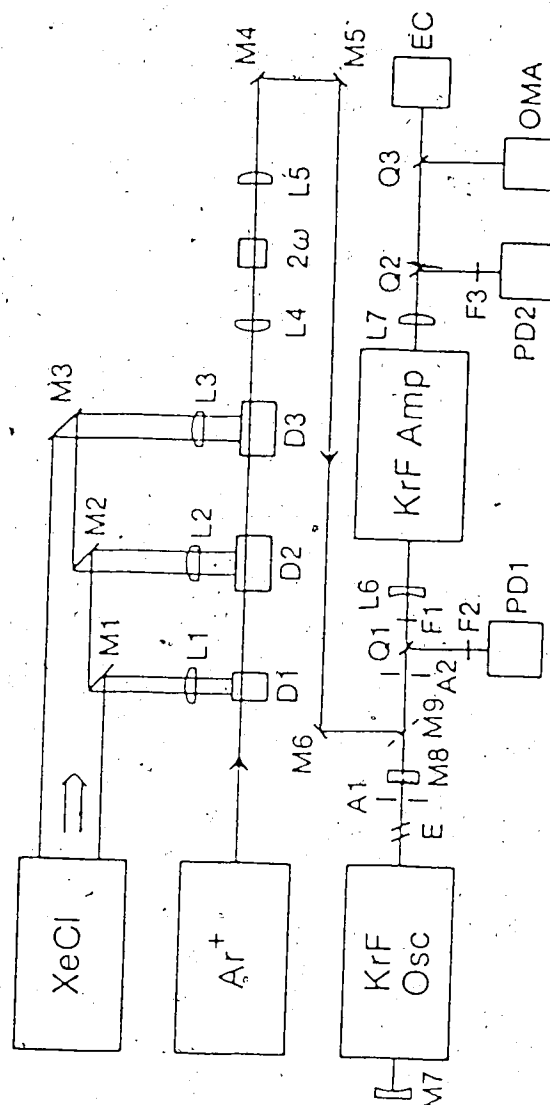
Fig.9 Experimental layout using both an etalon tuned KrF
oscillator and a frequency doubled argon ion laser source
for small signal gain versus wavelength measurements.

Experimental layout: A1-A2 - apertures, Ar$^+$ - argon
ion laser, D1-D3 - Coumarin dye cells, E - tuning etalons,
EC - energy calorimeter, F1-F3 - calibrated fillters, KrF
Amp - discharge amplifier module, M1-M9 - mirrors, OMA -
monochromator & optical multichannel analyzer, PD1-PD2 -
biplanar photodidodes, Q1-Q3 - quartz beam splitters, 2ω -
frequency doubling crystal.

the experiments two tuning etalons were inserted intracavity in the oscillator giving a measured output laser linewidth of ~ 10 GHz. Under these conditions an output power of several kilowatts in a 10 ns pulse was obtained from the oscillator. Either the frequency doubled argon ion radiation or the tunable oscillator radiation could be selected as input to the amplifier by the insertion of a removable mirror which was located at the entrance of the A1 laser module, as shown in Fig. 9.

The KrF amplifier module has a total accessible gain cross-section of 2.5x3.5cm with parameters as given in Table 1. However, only the central, relatively uniform, 1.1 cm diameter portion of the gain cross-section was probed in the saturation and small signal gain experiment. The discharge gain length of the particular amplifier module used for the present measurements was 96 cm. A gas mixture of He:Kr:F$_2$ = 0.896:0.10:0.004 was used at a total pressure of 1300 Torr. The measurements were made using a static fill of laser gas. Only results obtained in the first 30 shots after a gas refill were analyzed, during which time no signifcant degradation in gain was observed. The duration of the gain period was 24 ns.

In order to somewhat reduce the gain saturation, during the experimental measurements a divergent beam geometry was employed as shown in Fig. 10. A negative 273 mm focal length lens together with a 2 mm diameter aperture at the entrance to the amplifier module produced a circular diverging beam of full angle β = 7.32 mrad. Burnpatterns made on UV sensitive paper were used to obtain the spatial beam profile at
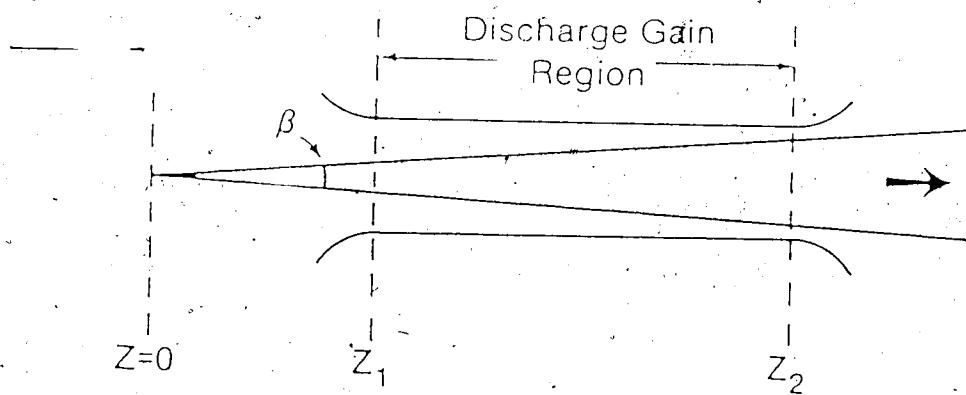
Fig. 10 The geometry used for gain and saturation measurements.

various axial points in the system indicating that the intensity was approximately uniform over the cross-section throughout the system. The end windows of the amplifier were tilted at Brewster's angle and lens elements were slightly tilted in order to prevent any back reflection of radiation into the amplifier module which could cause parasitic lasing. The output of the amplifier module was collimated using a 4 m focal length lens and then directed to the diagnostic monitors which were located approximately 5 m further away.

The main diagnostic measurement was a pair of cross calibrated photodiodes to measure the input and output power from the amplifier module. Sample photodiode traces are shown in Fig. 11 for both the frequency doubled argon ion and tunable KrF oscillator input. The input and output signals were displayed on the same oscilloscope trace, while the sweep was triggered from the electrical tri er used to fire the laser modules. The timing of the robe pulse relative to the peak gain time of the A1 laser module could be determined by the position of the photodiode traces on the sweep. Only those shots which indicated the input arriving during the peak of the 24ns gain period for the amplifier were analyzed to obtain he system gain. In order to measure the exact probe beam wavelength, the amplified output was also transported by a fiber to the entrance of a 57 cm focal length Ebert monochromator, the output of which was imaged onto an optical multichannel analyzer system. Overall spectral resolution was 0.03nm. The frequency doubled argon ion laser line was used for absolute spectral calibration of the system to an accuracy of 0.01nm.
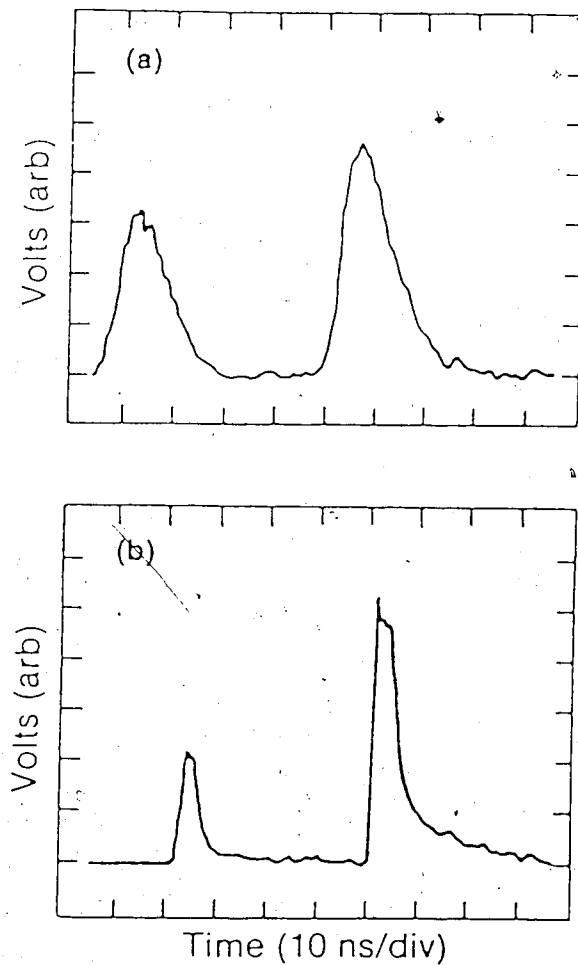
Fig. 11 Oscilloscope traces of the input followed by the output
photodiode signals for the small signal gain and
saturation measurements, (a) for the tunable KrF source
and (b) for the argon ion source.
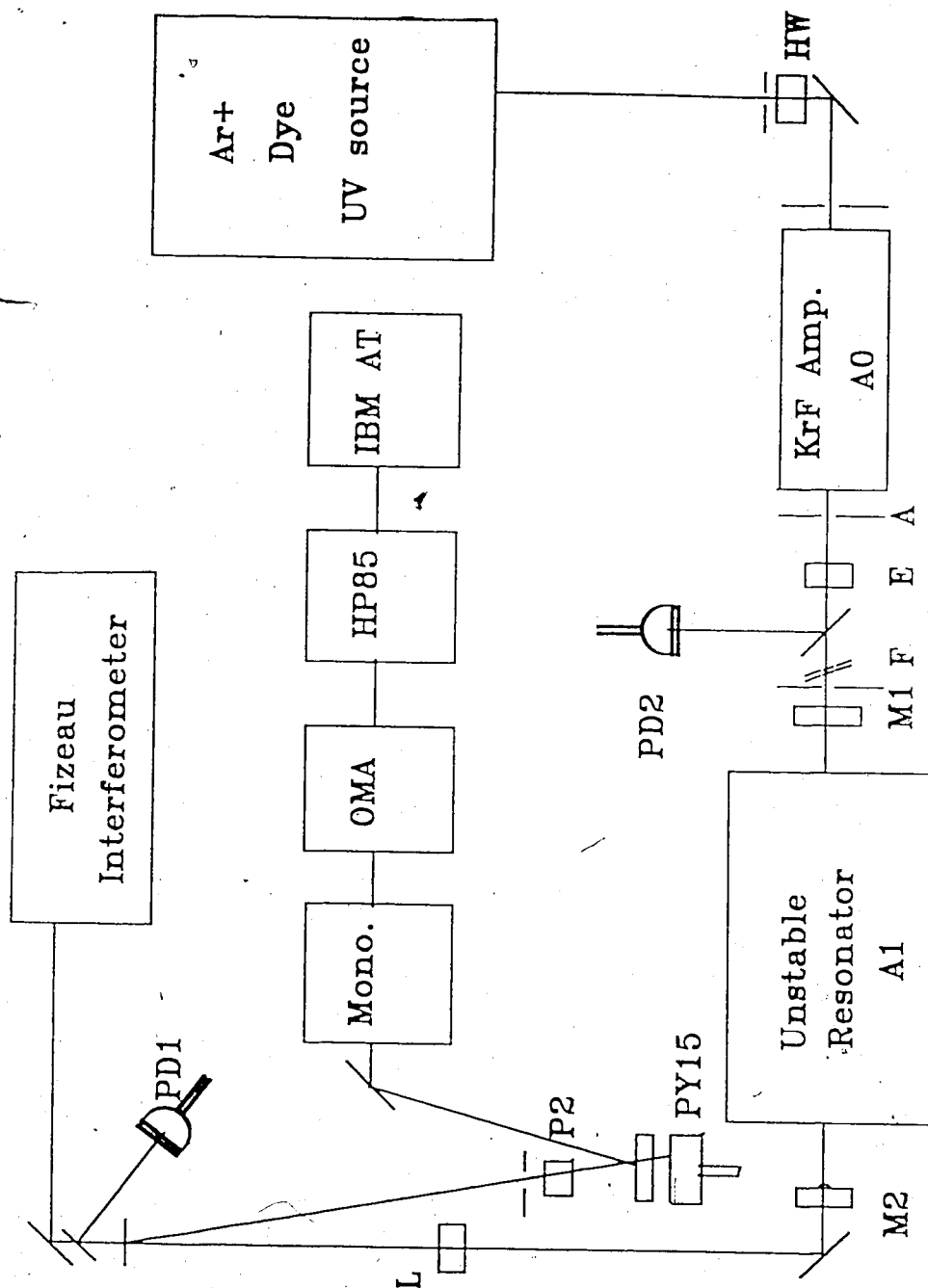
Fig. 12 The experimental setup for the injection locking measurements.

Experimental layout: A – aperture, E – etalon, M1–90% reflective mirror, M2 – meniscus mirror, , P2 – polarizor, AO–A1 – discharge KrF laser module, PD1–PD2 – biplanar photodidodes, PY15 – energy calorimeter, F – calibrated filters, HW – half wave plate, L–collimating lens.

3.4. Injection Locking Experiments

The layout of the injection locking experiment is shown in Fig. 12. In these measurements, the former master oscillator module was now used as a single pass KrF amplifer which amplified the argon ion generated UV pulse. This system could provide powers up to 10^4 W. The overall system alignment was very critical for all the injection measurements, directly affecting the efficiency of injection and the output beam polarization of the unstable resonator KrF laser amplifier. The polarization was affected since the beam path involved a beam periscope and a number of 90° turning mirrors. If the beam path was not square to within $\sim 2^\circ$ on these mirrors significant depolarization of the beam would occur. Throughout the measurements, the small KrF amplifier module, A0, was turned on and off in order to obtain higher and lower injection power. The agreement of the results using nonamplified UV and amplifed UV output power was checked for intermediate injection powers.

The 0.1mm air spaced etalon following the single pass amplifier was used to block ASE from the amplifier module and was removed when the oscillator was turned off in order to reduce the absorption losses. The measured transmissivities of the quartz beam splitter used for diagnostic purposes and the etalon were 84% and 34.5% respectively. The 15% reflection of the UV light from the quartz plate was monitored by photo diode PD2. The signals on PD2 were used to measure the input power into the A1 module and to check the timing between UV injection and the gain period of module A1. The etalon was set at a small angle

to avoid spontaneous oscillations in both laser modules. A 2mm diameter pinhole, A, was inserted in the laser beam after the etalon and prior to the diagnostics to give an accurate measurement of power injected into the unstable resonator, A1.

In front of the aperature the full UV laser spot was approximately 4mm diameter. After A1 the amplified UV light was split into several parts for the various measurement diagnostics. The output energy was measured using a pyroelectric calorimeter; the output power, pulse shape and timing using a biplanar vacuum photodiode; and the output spectrum using a monochromator system and a Fizeau Interferometer System.

A 0.57 M Ebert monochromator coupled to an optical multichannel analyzer (OMA) was used for the broadband spectral measurements. The main function of the system was to measure the fraction of output power in the narrow output linewidth as compared to the total output power. The spectra were captured and stored on a Hewlett Packard model 85 computer and then transferred to an IBM AT computer for data processing. An example of a resultant spectrum from this system is shown in Fig. 13. The spectral data was processed by smoothing the data and then subtracting the background signal. As shown in Fig. 13 the integrated broadband ASE signal was determined and subtracted from the total signal leaving the narrow linewidth component. The ratio of the narrow-linewidth to total area was then calculated to give the percentage injection locking for a given shot.
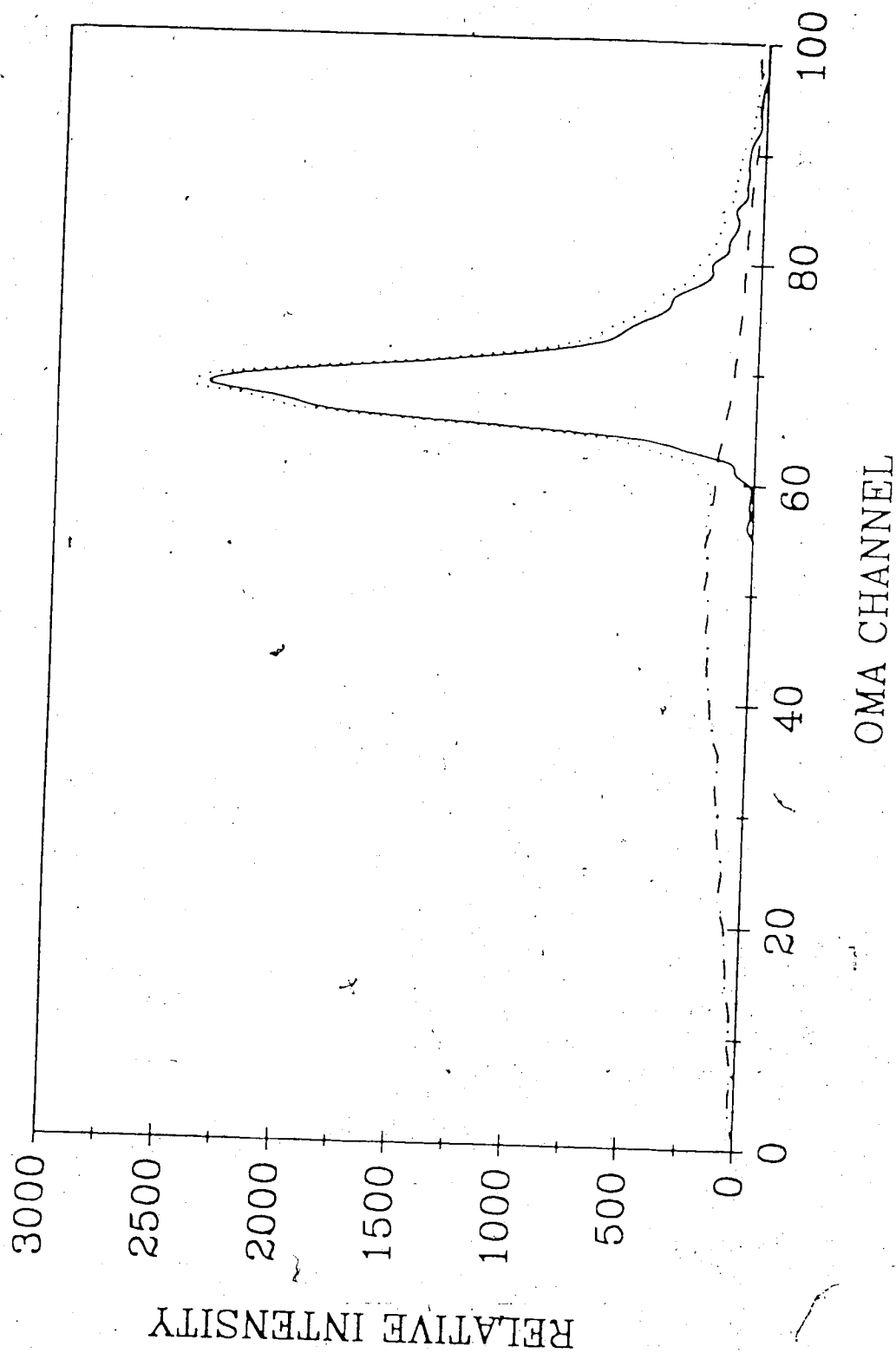
Fig. 13 A typical output spectrum including broadband ASE and injected narrow bandwidth output. The raw experimental data is given by the dotted line.

37

3.5. Diagnostic Systems

The main diagnostics used for the present experimental measurements consisted of cross-calibrated photodiodes, pyroelectric energy calorimeters and a monochromator/OMA system. The pyroelectric energy calorimeters were home made units with active areas of 2cmx2cm or 5cmx5cm and were cross calibrated to an accuracy ±5% with a Gentec Model ED-200 calorimeter. The photodiodes were Hamamatsu model R-1193U biplanar vacuum photodiodes with 300 ps rise times and were calibrated using beam splitters and filters to an accuracy ±10% against the above energy monitors. These calibrations were carried out at a wavelength of 248nm. The energy calorimeters had a resulting absolute accuracy of ±10% which together with errors of ±10% in beam cross-sections led to an overall experimental uncertainty of ±15% in beam intensities. The photodiodes were also cross-calibrated relative to each other in their respective measurement positions with the KrF laser modules turned off and evacuated. Calibrated filters were then employed in front of the photodiodes, as required, to maintain the signals within the linear range of the photodiodes. For the small signal gain measurements the measured intensities, taken from the peak of the photodiode signals, were corrected for losses in all optical elements in the beam path in order to give the true intensities at the entrance and exit of the gas medium in the amplifier module. For the single pass gain measurements the possible contribution of ASE light to the output signal was determined by observing the output signals with the input beam blocked. The level of ASE observed in this case was less than 10% of the weakest signal recorded and thus could be neglected.

As mentioned earlier a monochromator-OMA II system together with an IBM AT computer were used for spectral analysis. The OMA – II detector head was a silicon intensified two dimensional detector (EG&G, PAR, model 1254E), with a UV scintillator coating applied in order to obtain response at 248nm. The output of the 57 cm Perkin Elmer model E-1, monochromator was imaged with a magnification ratio of 3.5 times onto the OMA detector. The dispersion of the combined system using a 2880 line per mm UV grating was 0.00546nm/OMA channel.

For the injection experiments a narrow linewidth reference signal for calibration purposes was obtained from three different sources; the Brillouin backscatter radiation from the generation stage (B1 in Fig.5), a UV mercury lamp (253 nm) or the direct frequency doubled output of the argon ion /dye amplifier system. A reference signal was recorded once or more during each day's experimental run in order to determine the level of scattered light signal on the OMA detector outside of the narrow linewidth signal. The results of these reference measurements indicated a background scattered light level equivalent to 4% of the narrow linewidth peak. A correction factor was applied in the analysis of the data to account for this amount of scattered background light.

The OMA linearity was determined using calibrated filters and a fixed energy source: either broadband KrF laser radiation or narrowband SBS radiation from the Brillouin generation stage B1 (see Fig.5). It was found that the OMA output was not linear with
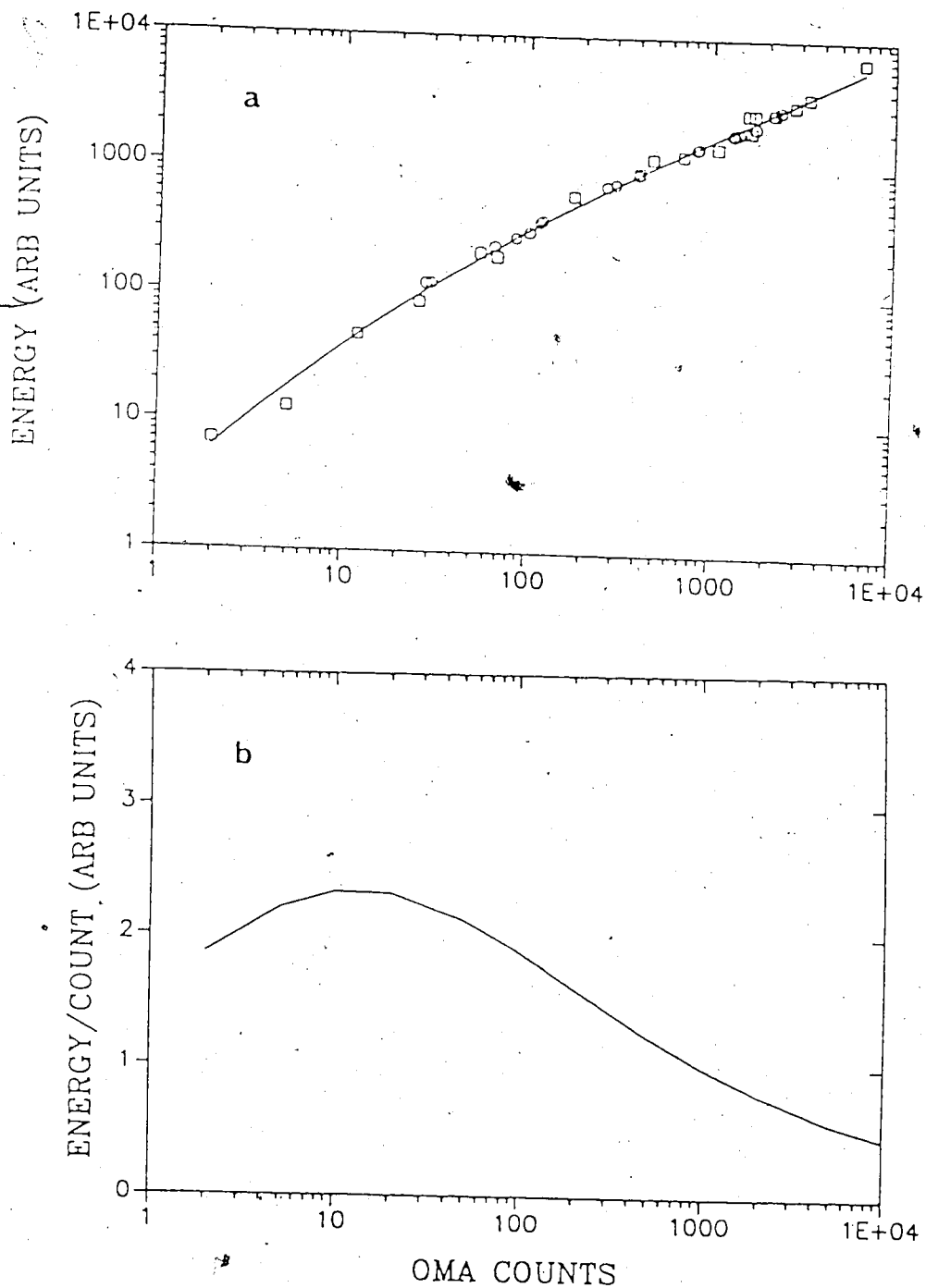
Fig 14 OMA linearity calibration : (a) Measured input power as a
function of OMA counts using broadband KrF radiation (o)
and narrowband KrF radiation (□); (b) Relative response as
a function of output counts.

illumination intensity for low intensity levels, as shown in Fig. 14 (a). From the measured response a correction factor was calculated to give the correct intensity for a given level of output counts as shown in Fig. 14 (b). This correction factor was applied to the data in the analysis procedure in order to compensate for the nonlinearity of the OMA system.

CHAPTER 4

EXPERIMENTAL RESULTS AND DISCUSSION

4.1. Argon/Dye/UV laser system

The argon ion laser was normally adjusted to deliver 51mW of ultra-narrow linewidth power at the entrance of the first dye laser amplifier. This value was chosen to stay well below the damage threshold ($10W/cm^2$) of the optical switch. The power at the entrance of the electro-optic switch was 150mW but since the electro-optic switch was previously damaged the transmission with voltage applied was less than 100%. In addition, the following polarizer and lenses were not anti-reflection coated resulting in an overall transmission of 34% from the entrance of the pulse switch to the entrance of the first dye cell.

As shown in Fig. 8, a three stage dye laser amplifier was employed for amplifying the weak input signal to moderately high intensities. Because of the large amount of amplification required for the weak input signal the amplifier stages were designed for high gain. Consequently, they did not operate at high efficiency.

The output power of each dye amplifier stage was measured as a function of the input argon ion laser power. The results are plotted in Fig. 15. The typical operating power level is listed for each stage in Table 2. The amplification factor of the first dye stage is approximately 1800 times with lower amplification factors in the

42
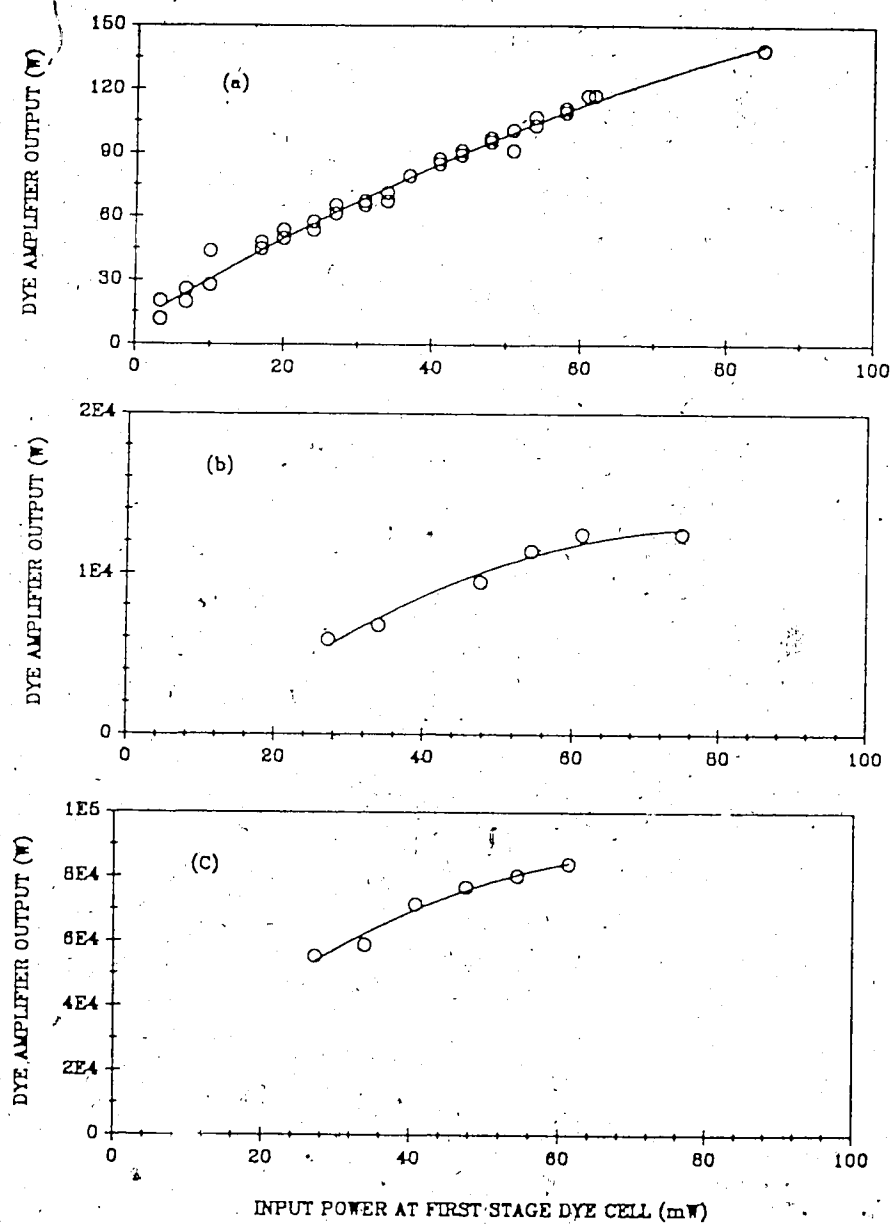
Fig. 15. The output power of different dye cell stages as a function of n ion laser input power at the first stage dye cell; (a irst stage dye cell (b) second stage dye cell (c) hir stage dye cell. The solid lines represent polynomial its to the data.

subsequent stages. These results are in agreement with the expected saturation of gain at high intensity for the second and third dye cells.

Table 2 Typical laser power at various stages

1. Argon ion laser output power (496.5nm)	150mW
2. Input power of the first stage dye cell (496.5nm)	51mW
3. Output power of the first stage dye cell (496.5nm)	92W
4. Output power of the second stage dye cell (496.5nm)	10.1kW
5. Output power of the third stage dye cell (496.5nm)	78kW
6. Output power of the Urea crystal (248.2nm)	2.5KW
7. Output power of the first stage UV amplifier (248.25nm)	10kW

In order to characterize the dye amplifier system so that it could be optimized in the future a number of measurements were made of the operating parameters. The measured dye laser ASE output spot sizes were, 1.2mm, 0.20mm and 0.11mm just after the first amplifier for dye concentration of 1×10^{-3} mol, 1×10^{-2} mol and 1×10^{-1} mol respectively as shown in Fig. 16. The measurements were made by moving a 50 μm slit across the exit face of the dye cell at a distance of 2mm from the cell. The output ASE sizes when corrected for geometric factors gave usable gain cross-sections of 0.86mm, 0.18mm and 0.067mm. The output beam size as measured here gives the effective depth of the XeC' pumped gain region which can then be used to optimize the concentration of

each dye cell for the beam size of the amplified narrow linewidth pulse.

The input argon ion beam spot size at the first dye amplifier stage was 178 μm (from the telescope design data, see Appendix A), which was bigger than the measured gain region of the first dye amplifier stage. Thus the amplified laser beam divergence and beam spot size are determined by the size of the gain region pumped by the XeCl laser. The dye amplifier cross-section was chosen to be smaller than the beam cross-section at each stage in order to ensure overfilling of the gain volume. This had the two effects of reducing the ASE signal since all the gain medium was extracted, and of making the alignment through the dye laser system less critical.

In order to facilitate alignment of the laser system the dye solvent mixture was adjusted (95% dioxane and 5% methanol) to give a peak amplified spontaneous emission (ASE) wavelength of 487nm. Since the peak wavelength shifts towards the blue end of the spectrum as the concentration of dioxane is increased the blue ASE output provided a contrast to the green amplified argon ion signal for ease of aligning the system.

When operated at a high input power level of 70mW into the first dye cell a peak output power of 84 KW was obtained at 496.5 nm. Normally, in order to prevent optical damage (to the Pockels cell, exit face of the final dye amplifier and turning mirror after the exit of
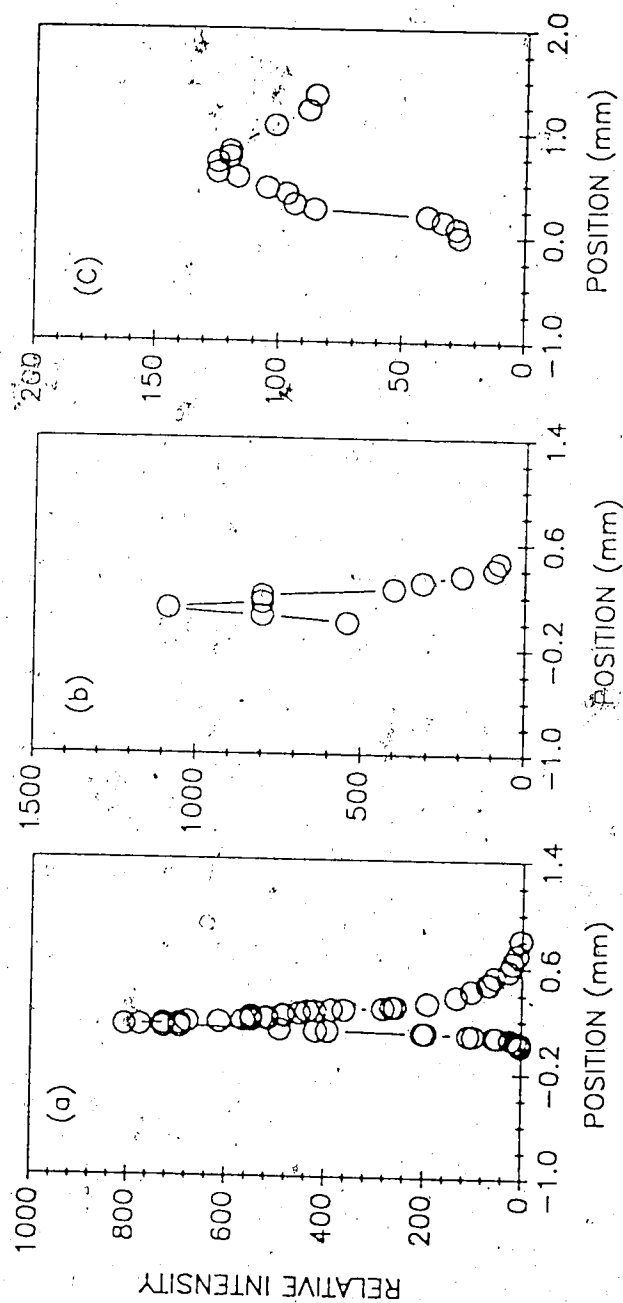
Fig. 16. The ASE beam spot size measurements of the first stage
dye cell at three dye concentrations; (a) 1×10^{-3} mol
(b) 1×10^{-2} mol and (c) 1×10^{-1} mol.

level of 78KW with an input signal of 51mW.

The output radiation was subsequently focussed through the frequency doubling crystal, type I Urea. The cone angle of the incident radiation was ~ 10mrad (5mm diameter beam, 500mm focal length lens), with the input face of the crystal located approximately 80mm before the focus of the beam, thus making the crystal less sensitive to angular alignment. The measured output power is plotted in Fig. 17 (a), as a function of input argon ion laser power; it reached a peak of 2.8KW at 70mW input power implying a conversion efficiency of 3.5%. The variation in output power as a function of tuning angle is shown in Fig. 17(b) giving a tuning range of ~ 14mr in approximate agreement with the incident focal cone.

4.2. Saturation and Small Signal Gain Measurements

Using the tunable oscillator and argon ion laser source, measurements of single pass amplification in a KrF laser module were made with a number of input intensities, and at several wavelengths. Because of the limited free spectral range of the tuning etalons employed in the oscillator, the range of available wavelengths was limited to the peak gain region of the KrF transition. Single line output was observed on the spectral monitor system over the wavelength range of 248.2 - 248.4 nm. Approximately 5 shots were taken for each input intensity and wavelength combination and the results averaged together. The complete set of results is tabulated in Table 3. All the
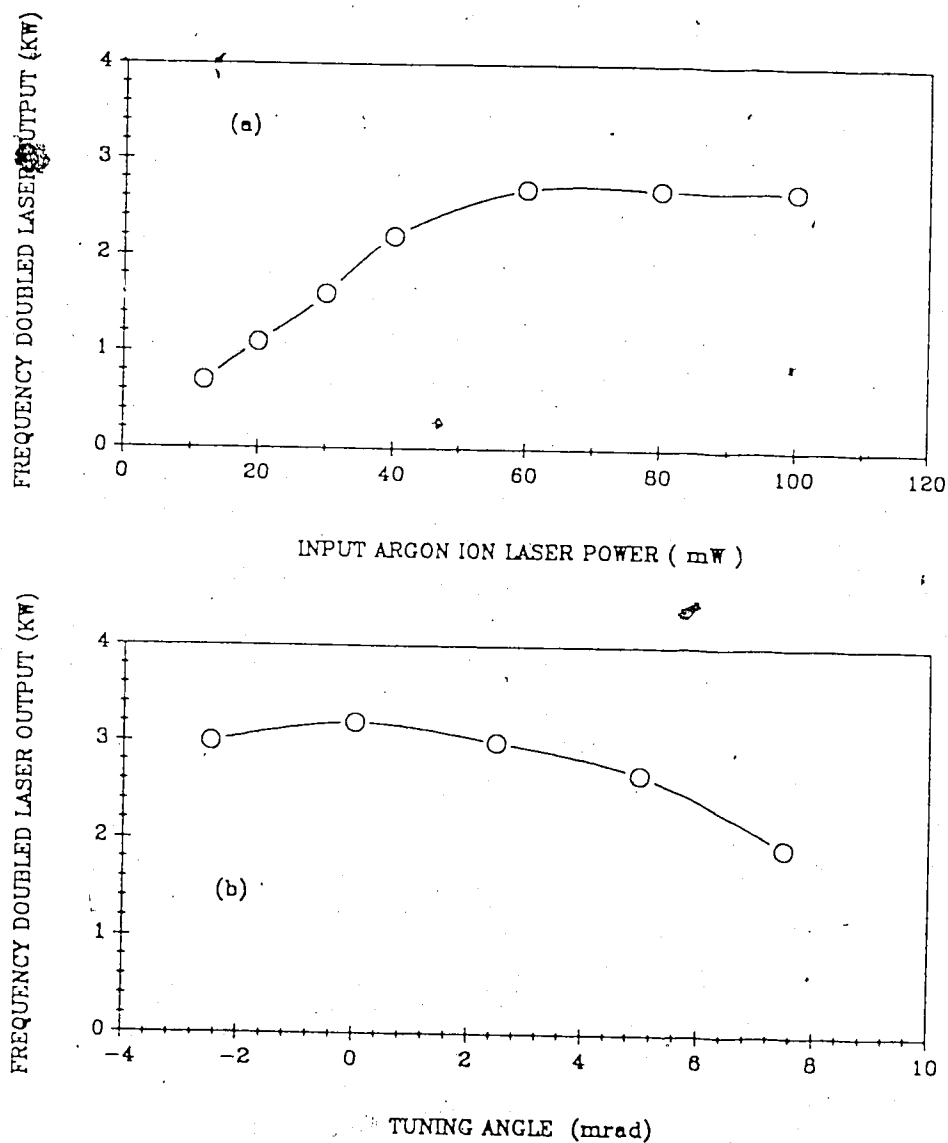
47

Fig.17 (a) Output power of the frequency doubling crystal as a
function of the argon laser input power.
(b) the output power of the frequency doubled light as a
function of Urea crystal angle tuning

resulting data points are shown plotted as a function of input power in Fig. 18. Saturation of the output power is clearly observed as the input intensity is increased.

Table 3. Measured Output Power as a Function of Input Power

λ_0 (nm)	P_{in} (W)	P_{out} (MW)	λ_0 (nm)	P_{in} (W)	P_{out} (MW)
248.22	15.9	1.58	248.31	219.6	3.83
248.22	218.7	4.13	248.32	19.0	1.94
248.25	2.5	0.48	248.32	154.4	3.12
248.25	12.1	1.41	248.40	11.7	1.33
248.25	32.2	2.70	248.40	15.8	1.53
248.25	213.9	3.87	248.40	225.9	3.82
248.31	15.5	1.52			

In order to determine the variation in gain as a function of wavelength, a model for the gain saturation has been used. In the model it is assumed that the laser line is homogeneously broadened and that the duration of the gain period and the input pulse lengths are long enough for the population inversion to reach its steady state value. Using these assumptions and keeping in mind the divergent beam geometry for the measurements, as shown in Fig. 10. one can write down the equation for the spatial rate of growth of the total power in the beam,
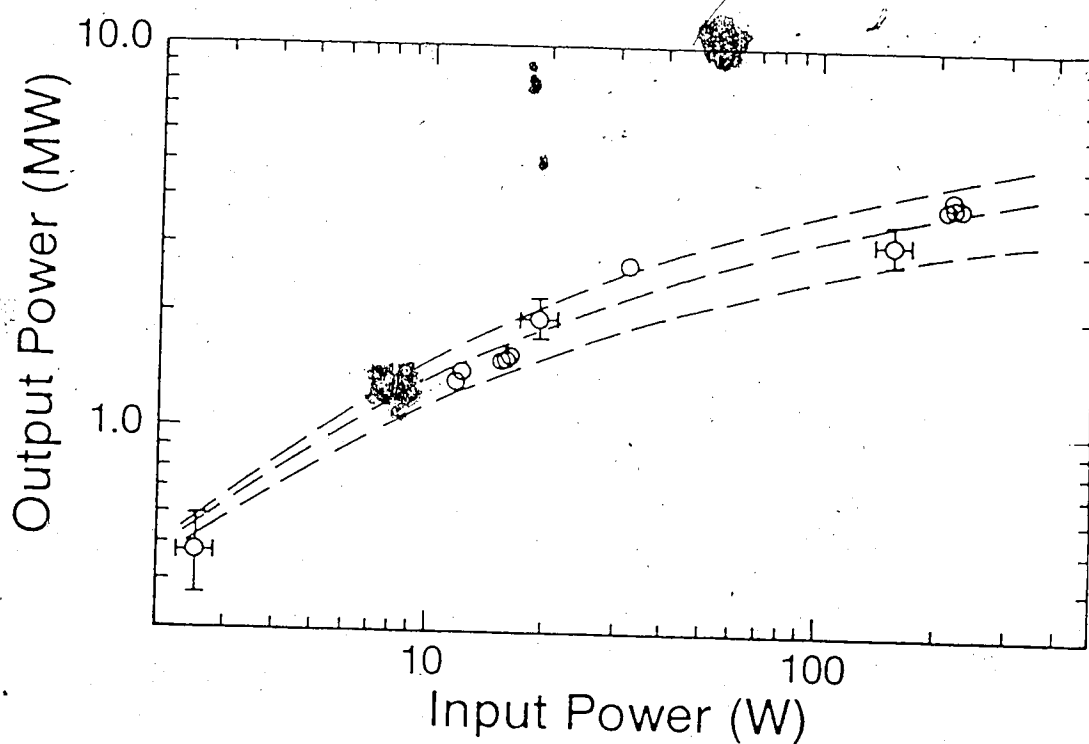
Fig. 18 The output power vs the input power for the saturation and small signal gain measurements. The three dashed lines represent the theoritical curves for I_s = 1.7 MW cm^{-2}, 2.3 MW cm^{-2} and 2.9 MW cm^{-2} all for small signal gain of g = 0.142 cm^{-2}.

P, as follows:

$$\frac{dP}{dz} = P\left[\frac{g^o}{1 + \frac{4P}{\beta^2 z^2 I_s}} - \alpha\right]$$
(4.1)

where g is the small signal gain per cm, α is the nonsaturable loss per cm, β is the full divergence angle of the expanding circular beam cone, I_s is the saturation intensity, and z is the distance from the imaginary point source of the input laser beam.

The above differential equation was solved on a computer using a fourth order Runge-Kutta technique for various values of g and I_s. The input pulse started at z_1 = 45cm and the amplification was calculated up to the point to z_2 = 149 cm, corresponding to the parameters for the gain medium in the experiment. Because of the difficulty in measuring the nonsaturable absorption, α, the value is taken to be 0.01 cm^{-1}, as measured for a similar KrF discharge laser [29]. The best fit to the complete set of experimental data was obtained with a gain and saturation value of g = 0.142 ± 0.002 cm^{-1} and I_s = 2.3 ± 0.3 MW cm^{-2} as shown in Fig. 18.

To compare the gain and performance for the various wavelengths an average saturation intensity was assumed and the best fit gain for each measured wavelength was calculated. It was assumed that the saturation intensity was fixed at I_s = 2.3MW/cm^2 for all wavelengths

within the gain region. With this assumption the gain corresponding to each input wavelength could be found by fitting to the measured amplification factors. The various values obtained from different input intensities for each wavelength were averaged together to give an average gain for each wavelength.

The resultant values of the gain are shown plotted in Fig. 19. In the graph the measured gain ranges from the highest value of $g = 0.143$ cm^{-1} at the wavelength of 248.2 nm to the value of $g = 0.141$ cm^{-1} at the wavelength 248.4 nm. In our experiment the fact that the KrF oscillator hops to the next wavelength mode as the etalons are tuned to wavelengths shorter than 248.2 nm or wavelengths above 248.4nm indicates that the gain must fall off for both shorter and longer wavelengths than the measurement range .

The gain was also measured using the frequency doubled argon ion laser source; it turned out to be equal to the peak gain of 0.143 cm^{-1}. From the observed ASE spectrum (see Fig. 13) the peak ASE signal occurs at a wavelength of 248.34nm which indicates that the peak gain occur at this wavelength. Thus the best overall fit to the gain profile s estimated to follow the dashed line shown in Fig. 19. Within e experimental error of ±1.5% it appears that the gain at the freque doubled argon ion wavelength is essentially equal to the peak gain. Thus, it appears that the argon ion wavelength is well matched for injection locking and subsequent amplification in a large multi-stage KrF laser system.
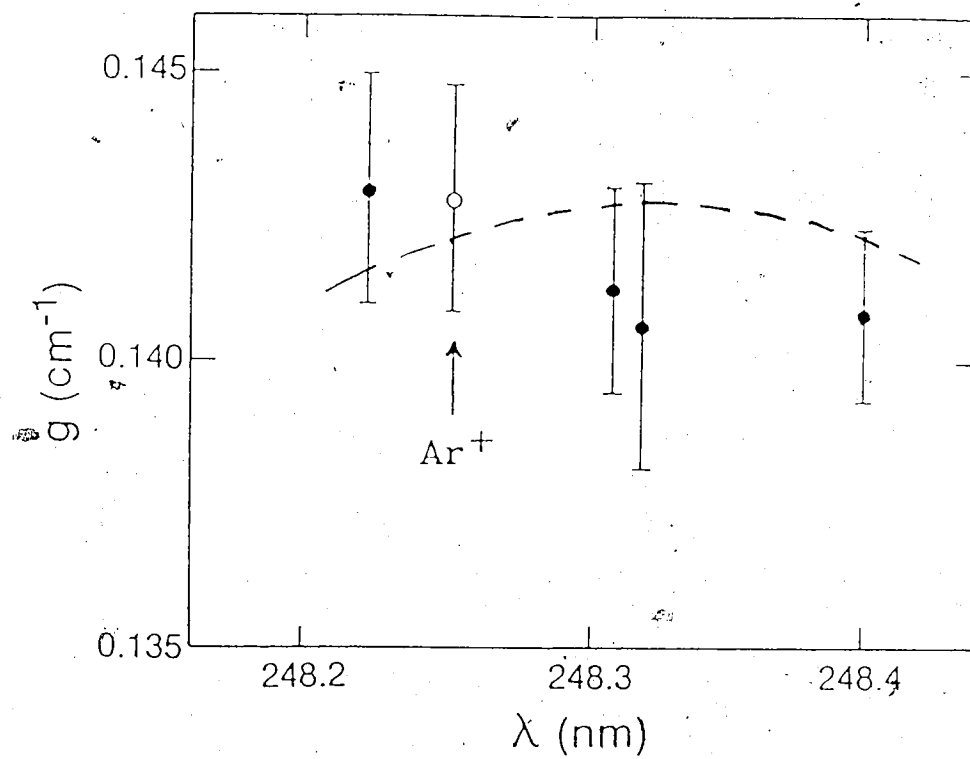
Fig. 19. Small signal gain as a function of wavelength.

4.3. Injection Mode Locking Measurements

Since the pulse duration of our frequency doubled argon ion radiation was too short (~ 3.5 ns) to obtain complete injection locking of the A1 module output, an optical delay system was used after the the Urea crystal to double the pulse width (see Fig.8). The typical photodiode traces of the UV input and amplified laser pulses for the injection measurements are shown in Fig. 20. The pulse durations are 3.5ns and 6.5ns with and without the pulse stacker respectively. The short 3.5ns injected pulsed is too short to fill one complete round trip of radiation in the unstable resonator, which requires 10.7ns, and thus part of the laser mode still builds up from spontaneous broadband emission. In contrast, the longer pulse, 6.5ns , is sufficient to lock most of the output radiation. However, because of the difficulty in aligning the pulse stacker no attempt was made to go to a pulse tripler system to give complete input injection.

A series of traces of the raw output spectrum is shown as a function of injection power in Fig. 21 for the 6.5ns long injection pulses. The injected signal is varied by changing the neutral density filters shown in Fig. 12. The input power is defined as the power entering the 90% rear reflector of the unstable resonator module which falls within the diameter of the meniscus mirror upon exiting the unstable resonator. With zero injection, the unstable resonator produced a broadband output signal. The injected signal competes with amplified spontaneous emission for low injected powers levels. The narrow linewidth component is too narrow to be resolved by the

54
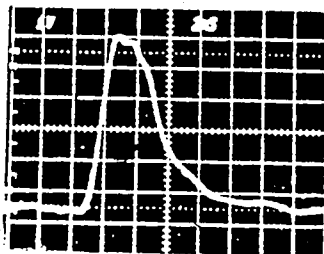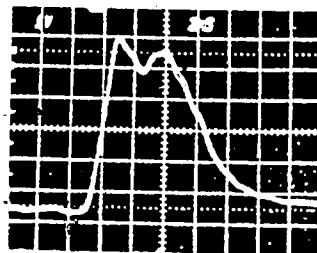
(a) 2ns/div   (b) 2ns/div
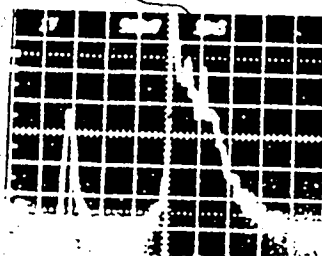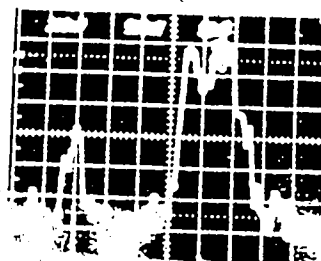
(c) 10ns/div   (d) 10ns/div

Fig. 20 Photodiode traces of UV input (a),(b) and amplified laser pulses (c),(d) for injection measurements, for the 3.5ns pulse (a),(c); and 6.5ns pulse (b) and (d).
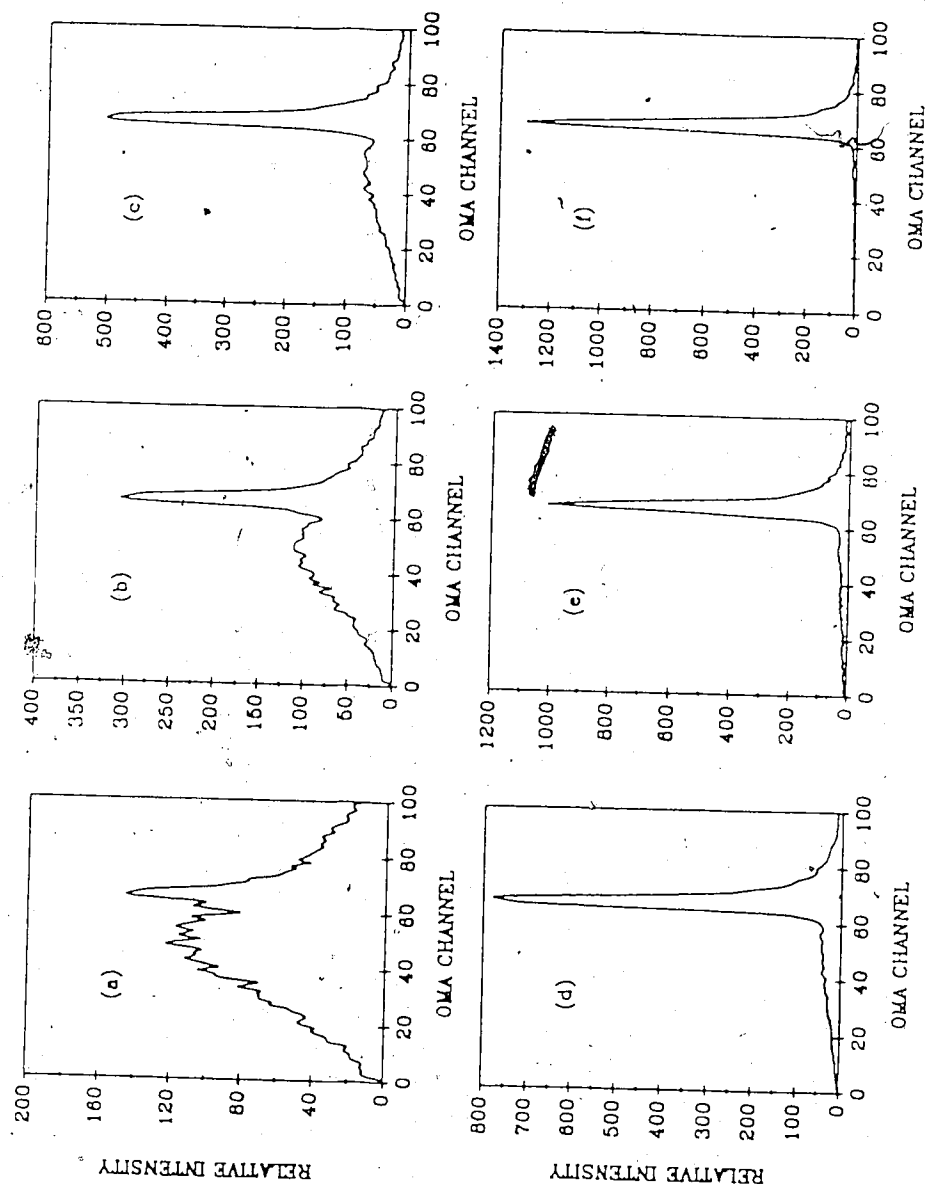
Fig. 21 Measured output spectra as a function of input power to
unstable resonator; (a)11% injection for 0.15W input
power. (b) 19% injection for 0.33W input power. (c) 36%
injection for 1.4W input power. (d) 56.% injection for
4.4W input power. (e) 80% injection for 232W input power.
(f) 91% injection for 335W input power.

monochromator/OMA system and thus appears on the output trace with an instrumental linewidth of 0.03nm. However the energy in the narrow linewidth component is still given by the area under the instrumentally broadened curve. The percentage injection locking is defined as the ratio of the area for the narrow linewidth component to the total area under the spectrum. As can be seen from the traces, above 10W injected power, the output of the high energy oscillator is forced almost totally into the 100MHz linewidth of the frequency doubled argon ion laser line.

Another critical factor in the injection locking process is the timing of the injection pulse, particularly if the pulse duration is only the length of one cavity round trip. Normally the beam should be injected into the unstable resonator concurrent with the initial rise of gain in the unstable resonator and should last until the stimulated mode in the unstable resonator is well above the spontaneous emission level. The optimum timing was determined by setting the injection signal at a relatively low fixed level and varying the time of the input pulse relative to the gain peak of the unstable resonator. The resulting measured percentage injection of the output is plotted as a function of time in Fig.22. As can be seen the time window for optimum output locking, i.e. > 90% of the peak, is on the order of 9ns.

In order to deconvolve the residual amount of ASE light remaining for high input injection signals it was necessary to correct for scattered light within the monochromator/OMA system. To do so required
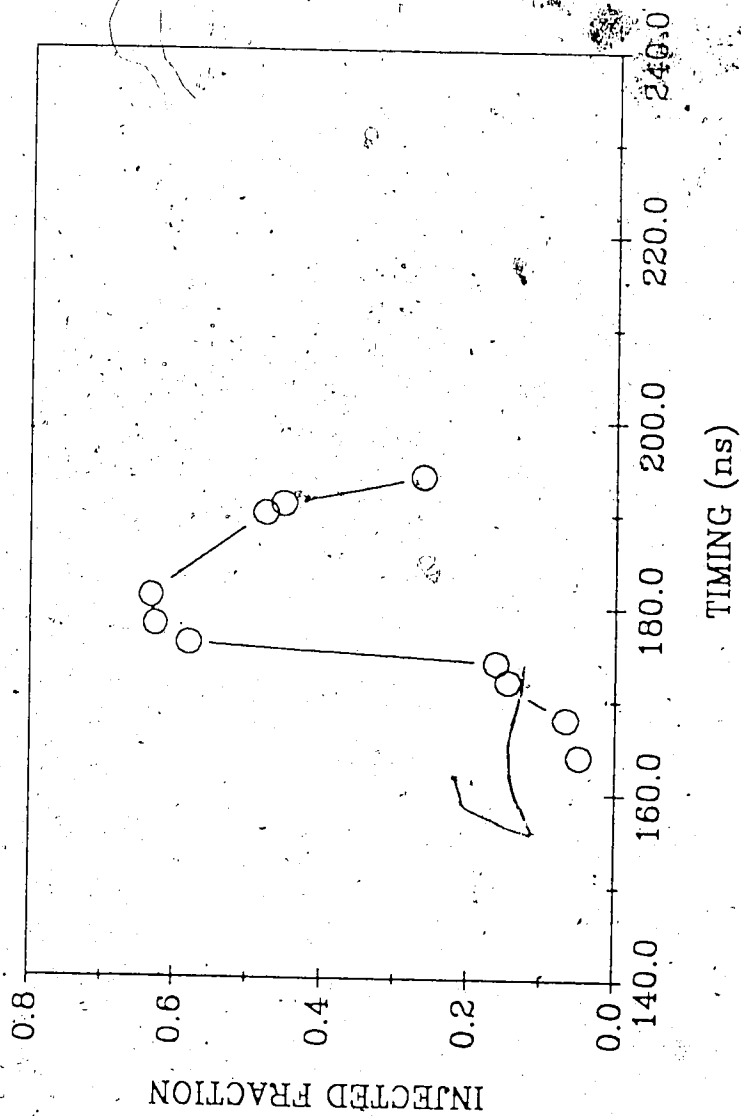
Fig.22 The percentage injection locking as a function of timing between the dye laser and KrF unstable resonator systems.

recording signals from known spectrally pure sources under identical measurement conditions. This was done using three different spectral sources which were: the Brillouin backscatter light from the generation stage of the optical pulse compressor system (see B1 in Fig.5), the pure second harmonic signal after the Urea frequency doubling crystal and the 253 nm line of a mercury calibration lamp. The resultant calibration spectra are shown in Fig.23. By analyzing these signals using the same technique as for the experimental data the backgroundsignal to narrow linewidth signal was found to be 95.8%, 95.8% and 94.0% in the three cases. Based on these residual background signals all the raw results were corrected by an average correction factor of 1.044 times in data processing. In addition, as described in the diagnostics section all the raw OMA signals were corrected for the nonlinearity of the OMA response.

With the above correction factors the injected fraction of the output signal was calculated from the measured data as a function of input injection power. The input injection power refers to the power at the entrance to the 90% reflective mirror, 0.1m, in Fig.12. In addition, only the part of the beam which interceped the meniscus mirror of the unstable resonator, 49.3% of the beam through the aperture, was counted in the input power. Thereafter the total transmission through the 90% reflective plane mirror, the Brewster polarizing plates and the calcium fluoride entrance window into the laser gas was 8.3%.
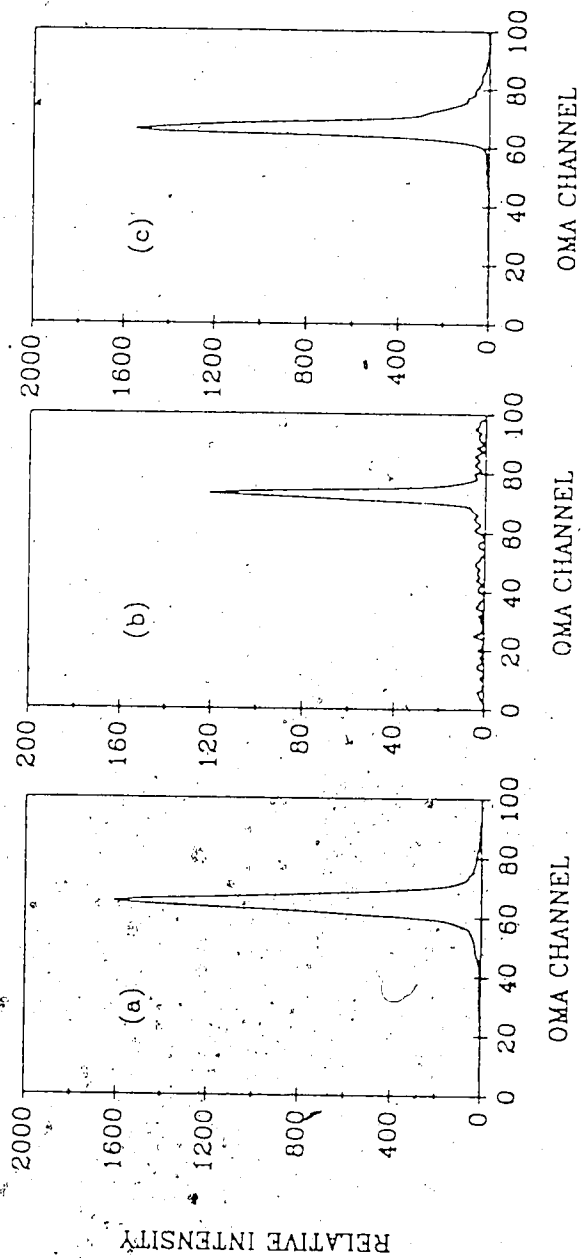
Fig. 23 The measured spectra of three spectrally pure light
sources.
(a). Mercury lamp
(b). The laser light after Urea crystal
(c). B1 light from the Brillouin compression system

The results are plotted in Fig.24 for the 3.5ns input pulse and
in Fig.25 for the 6.5ns input pulse. As can be seen with the longer
pulse the injection fraction reaches 80% at an input power of 100W and
falls below 20% at an input power of 0.3W. For the 3.5ns case the
injection locking never reaches 80% even at 10kW input power and falls
to 20% at an input power of 0.4W.

In both cases the injection fraction never reaches 100% even for
the highest input powers available. This is due to two factors.
First, the input pulse duration is not sufficient to completely fill one
round trip of the resonator. As can be seen, increasing from the
3.5ns to 6.5ns gives a marked improvement in the resulting output.
Secondly, with the given unstable resonator geometry, at the end of the
cavity by the flat mirror a large volume of the laser is not extracted
and it acts as a source of ASE which subsequently is amplified through
A1 and mixes with the injected output at the exit of the laser module.

Another important factor for injection locking is mode matching of
the input seed pulse and the injection locked cavity. This requires
matching of both the transverse and longitudinal modes. However, the
previous reports of the effects of accurate mode matching have dealt
with stable resonator geometries. When injecting into an unstable
resonator the detailed wavefront of the unstable resonator mode is very
complex and cannot be matched accurately using an injection source. In
this case best matching is achieved by matching the radius of curvature
of the seed pulse wavefront with that of the unstable resonator at the
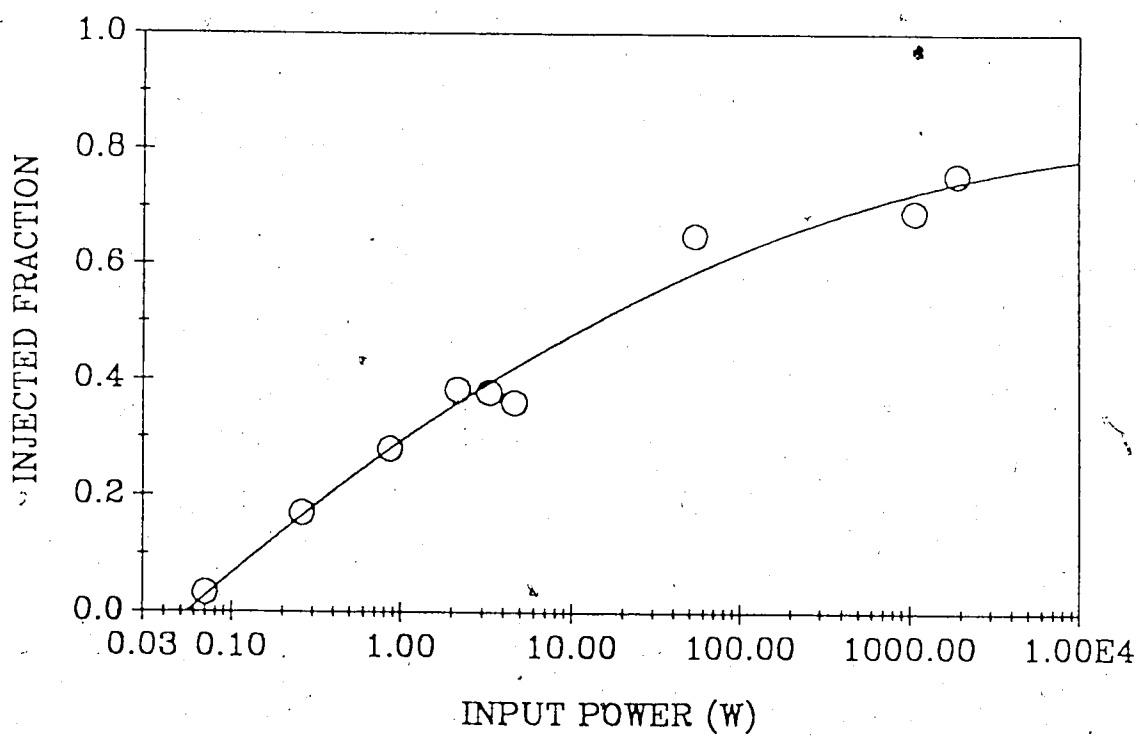
Fig.24 The unstable resonator injection spectrum using input radiation duration of 3.5ns. The solid line is a least squares polynomial fit to the data.
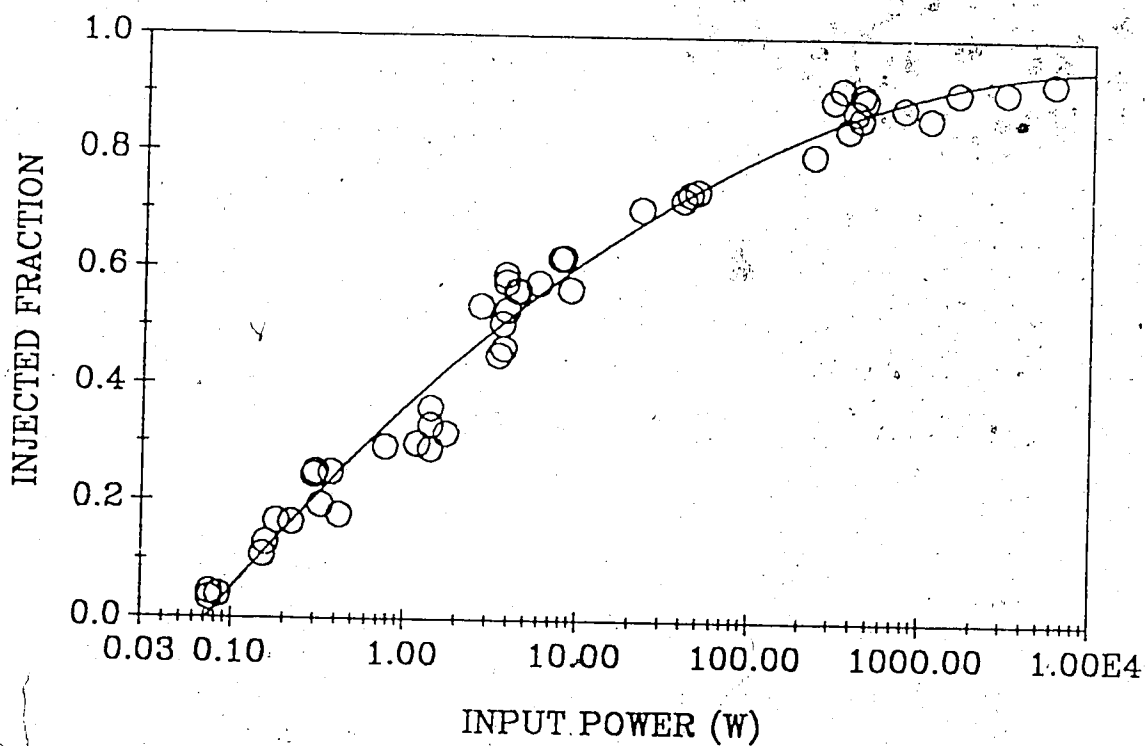
Fig. 25 The unstable resonator injection spectrum using input radiation duration of 6.5ns. The solid line is a least squares polynomial fit to the data.

position of the first mirror reflector [29], *i.e.* at the meniscus mirror in our case. The measured divergence of the UV injection seed beam gives a radius of curvature of 5.8M for the injection seed wavefront at the meniscus mirror. Following the equations given in reference [29] the unstable resonator mode itself has a wavefront curvature of 3.48M at this point. Using the criterion that good injection requires a wavefront matching of better than $\lambda/2$ after one round trip in the resonator, good injection can be achieved with input radii of curvatures of 0 to 9.2m [29]. Our injection wavefront curvature falls within this range and thus indicates reasonable matching.

Previous experiments with unstable resonator geometries have not established whether exact cavity length matching is important for unstable resonators. Certainly, such exact matching is important for stable resonator cavities [30]. In order to determine whether such cavity length matching is important in the present laser system is very difficult since the cavity length must be adjusted to a fraction of a wavelength. The optical mounts used in the present unstable resonator are not stable enough for such precise adjustments and it is estimated that the cavity length varied by a wavelength on a time scale of ten minutes. Thus it was not possible to attempt any systemati cavity length scanning. Instead, as a partial test of cavity length at ng the injection signal level and timing were fixed and 25 shots were taken in succession while adjusting the cavity length randomly by multiple wavelengths every four or five shots. It was expected that a

random distribution of cavity lengths was obtained by these means. If, as in the case of stable cavity geometries, a very large improvement in output injected power is observed when the cavity length is matched to within one tenth of a wavelength [30] it was expected that two to three shots should show very much improved output characteristics. The distribution of results is shown in Fig. 26. While there is some spread in the data, no exceptional shots were observed. Because of the slow transfer times of the data from the OMA system to the HP85 computer it was not feasible to take a larger number of shots in one day's run. The results, at least, are consistent with the expectation that longitudinal cavity modes are not well defined in unstable resonatorsand thus exact cavity length mathing is not critical under such conditions.

The output linewidth of the injection locked system was measured using a Fizeau Wedge interferometer system. The interferometer consisted of two 90% reflective mirrors separated by a distance of 29.1cm giving a free spectral range of 515MHz. The planar laser beam wavefront produced parallel fringes at the output of the interferometer which were adjusted to a spacing of about 4mm apart and viewed with a UV sensitive vidicon. The image recorded on the vidicon was captured using a video digitizer system and stored on floppy diskettes for subsequent analysis. A typical output spectrum showing two fringes is shown in Fig. 27. While showing some structure, as expected for such a Fizeau wedge interferometer system, the recorded linewidth is ~ 100MHz. However, a number of correction factors such as the linearity of the
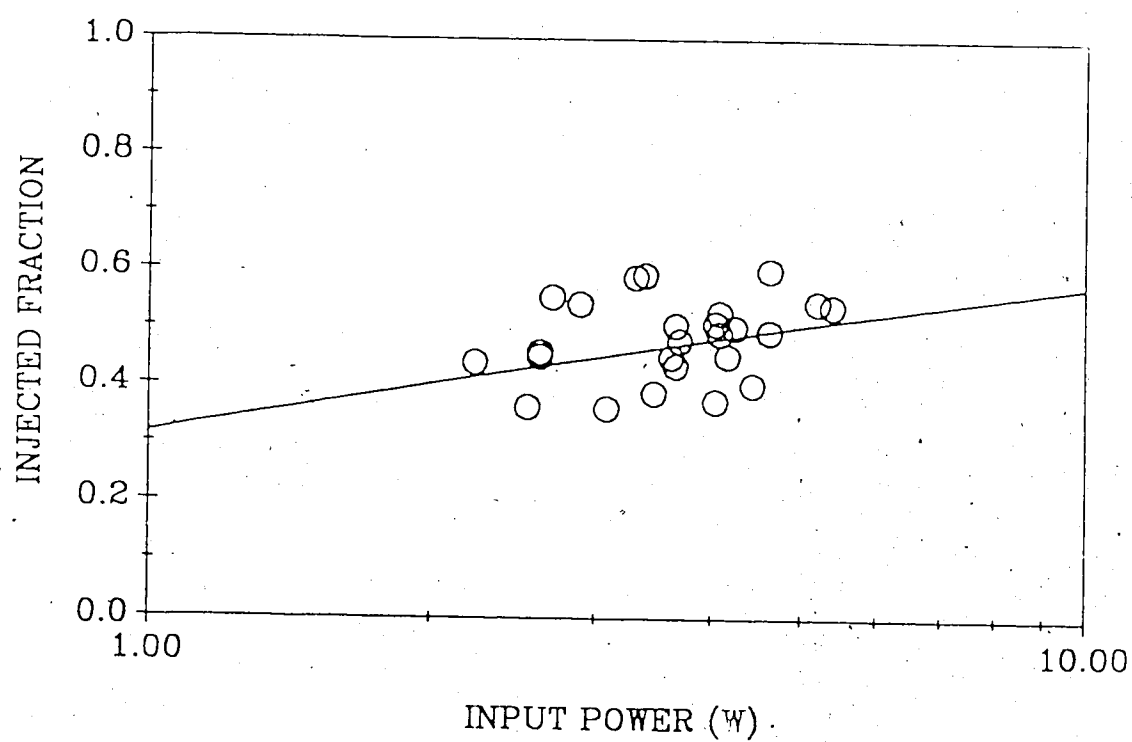
Fig.26 The injection vs input power for the cavity length
adjustment experiments; the solid line was taken from
Fig.25.

camera response, the accuracy of alignment of the incident laser beam
perpendicular to the interferometer plates, the theoretical
instrumental resolution and divergence of the input beam must be taken
into account in determining an accurate value or the true linewidth.
This more detailed determination is being carried out as part of
another student thesis project.

A comparision can be made between the results measured here and
previous injection locking experiments for KrF lasers. Goldhar and
Murray [26] used the output of one etalon tuned stable resonator module
to injection lock an unstable resonator module. They did not give
detailed measurements of percentage injection locking. However, basedon
the output spectra which they presented they required 500W of injected
power to achieve almost complete locking and 50W of injected power to
achieve ~ 50% injection locking. These powers are somewhat higher than
the present experimental results but the authors state that no attempt
was made to achieve mode matching or to optimize the unstable
resonator.

Bigio and Slatkine [9,18] reported almost complete injection
locking with 10W of power through a 1mm hole in the unstable resonator
mirror. At 0.1W injected power they observed injection locking on the
order of a few percent. Again, no quantitative numbers are given so
that it is difficult to compare with our results in detail. If we take
the 10% transmission of the entrance mirror in the present experiment
into account our measured values are comparable to Bigio and Slatkine's

Injection Locked KrF Oscillator Output

Free Spectral Range = 515 MHz
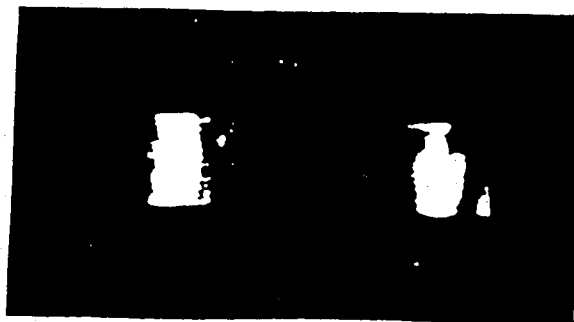
Linewidth ~ 100 MHz

Fig. 27   Fringe   pattern   measured   with   a   Fizeau   wedge
          interferometer system.

results. In their experiment they took great care to mode match and optimize the unstable resonator geometry which would indicate that the system used in the present experiment is also fairly well mode matched. Thus the injection locking results reported here appear to be comparable to the best reported results to date.

CHAPTER 5

CONCLUSION

An ultrahigh spectral brightness KrF laser system employing an argon ion laser source has been developed and studied. The system is characterized by reproducible linewidth characteristics and reliable operation. The laser system is ideally suited for applications in optical pulse ___ion where sources of ultra-narrow linewidth UV radiation a___ Experimental measurements have been made of the saturation intensity and variation in gain as a function of wavelength for the peak gain region of the KrF laser. The injection mode locked output of an unstable resonator has been characterized as a function of the injection input power.

This study indicates that the centre of the peak laser gain region is at 248.34 nm decreasing at both shorter and longer wavelengths. Within experimental accuracy the measured small signal gain at the frequency doubled argon ion laser line of 24ι 25nm is the same as the measured peak intrinsic gain. The measured peak gain was $0.143 \pm 0.002 \text{cm}^{-1}$ and the average saturation intensity was $I_s = 2.3 \pm 0.3 \text{ MW cm}^{-2}$.

It is also demonstrated in this study that there is a very low threshold, approximately 0.1W input power, for injection locking the unstable resonator. The input power required to achieve the maximum

70

output injection locking of 90% was measured as 1kW. Based on this work it looks very possible to obtain ~ >95% injection locking output using a longer pulse duration, >10ns, for the injected laser pulse.

For the ultrahigh spectral brightness KrF excimer laser system developed in the present thesis a number of more detailed measurements should be carried out in the future. Firstly, a detailed numerical model of the dye amplifier system must be developed in order to optimize the system parameters. Some of the experimental measurements required to provide the parameters for such a model have been carried out during the course of the present thesis work. This includes measurements of gain volumes, ASE output powers, dye fluorescence life time, and gain per stage for the three dye cell stages. Only some of these results have been included in the present thesis.

Next, a more detailed numerical model of the injection locking process is required. For this modelling there are only a few related papers on dye laser systems [31] and excimer laser systems [32].

Since the dye amplifier pulse duration presently available is too short to give total injection of the KrF unstable resonator, a longer pulse duration ~ 20ns source should be employed as the injection seed pulse in the future. To carry this out, the present XeCl laser should be replaced by a 20ns pulse duration XeCl laser as the pump source. In the event of such a replacement all the parameters for the dye amplifiers, for example, the pump focal lengths of the cylindrical

lenses, have to be very carefully readjusted. In particular, care must be taken not to exceed the damage thresholds on the dye cell windows and dye laser optical components.

Even after installing a longer pulsewidth dye source there may still be a contribution to the broadband output signal from the unextracted laser volume in the unstable resonator. In that case it may be desirable to replace the present unstable resonator geometry with a true confocal cavity. The latter geometry would ensure extraction of the complete laser volume on the output pass of the unstable resonator.

REFERENCES

[1]. M. Rothschild and D.J Ehrlich. "A review of excimer laser projection lithography." J.Vac.Sci. Technol. B6, pp. 1-17, 1988.

[2]. J.R.Murray, J.Goldhar, D.Eimerl and A.Szoke, "Raman pulse compression of excimer lasers for application to laser fusion."IEEE J.Quantum Electron., QE-15, pp 342-368, 1979

[3]. J.J.Ewing, R.A.Haas, J.C.Swingle, E.V.George and W.F.Krupke, "Optical pulse compressor systems·for laser fusion." IEEE J.Quantum Electron., QE-15, pp 368-379, 1979.

[4]. I.V.Tomov, R.Fedosejevs and D.C.D. McKen, "High -efficiency stimulated Brillouin scattering of KrF laser radiation in SF_6", Optics Lett. 9, pp 405-407, 1984.

[5]. R.Fedosjevs, I.V.Tomov, D.C.D. McKen and A.A.Offenberger, "Experimental study of an SF_6 Brillouin amplifier·pumped by KrF laser radiation," Appl. Phys. Lett., 45, pp340-342, 1984.

[6]. R.Fedosejevs and A.A.Offenberger, "Subnanosecond pulse from a KrF laser pumped SF_6 Brillouin amplifier" IEEE J.Quantum Electron., QE-21, pp 1558-1562, 1985

[7]. D.C.D.McKen, R.Fedosejevs, M.Arnfield, I.V.Tomov, C.Domier, and A.A.Offenberger. "Electrically triggered multimodule KrF laser system with narrow-linewidth output." Rev. Sci Instrum. 54, pp 845-852, 1983

[8]. R.G.Caro, M.C.Gower and C.E.Webb. "A simple tunable·KrF laser system with narrow bandwidth and diffraction-limited divergence"

73

J. Phys. D: Appl. Phys., 15, pp. 767-773, 1982

[9]. I. J. Bigio and M. Slatkine, "Attainment of the thoretical minimum input power for injection locking of an unstable-resonator KrF laser" Optics Letters, 6, pp 336-338, 1981

[10]. R. Fedosejevs, I. V. Tomov, D. C. D. McKen, M. Arnfield, C. Domier, and A. A. Offenberger, " Narrow-linewidth gain and saturation measurements of a KrF discharge laser", J. Appl. Phys. 54, pp 5629-5632, 1983

[11]. T. H. Johnson, "Physics of the krypton fluoride laser", J. Appl. Phys., 51, pp 2406-2420, 1979.

[12]. C. A. Brau, "Rare gas halogen excimers", Chapter 4 of "Excimer lasers", 2nd. ed., C. K. Rhodes, ed. Springer-Verlag, Berlin, 1984 J. Liegel, F. K. Tittel, W. L. Wilson, Jr., G. Marowsky, " Continous broadband tuning of an electron-beam-pumped XeF (C $\rightarrow$ A) laser", Appl. Phys. Letter. 39, pp 369 -371, 1981.

[14]. R. S. Hargrove. J. A. Paisner; in "digest of topical meeting on excimer lasers", IEEE Cat. No. 79, IEEE. New York.

[15]. R. T. Hawkins, H. Egger, J. Bokor, and C. K. Rhodes, "High spectral brightness excimer systems", in "Excimer Lasers" 2nd ed, C. K. Rhodes, ed, Spring-Verlag, Berlin, 1985

[16]. A. E. Siegman and H. Y. Miller, "Unstable optical resonator loss calculations using the prony method", Appl. Opt. 9, pp 2729-2736, 1970; A. E. Siegman, "Unstable optical resonator", Appl. opt. 13, pp. 353-367, 1974.

[17]. C. J. Buczek and R. J. Freiberg, "Hybrid injection locking of high power CO_2 lasers", IEEE J. Quan. Electron., QE-8,

pp.641-650,July 1972; C. J. Buczek, R.J.Freiberg, and M.L.Skolnik, "laser injection locking", Proc. IEEE, 61, pp. 1411-1431, 1973

[18]. I. J. Bigio and M. Slatkine, "Injection-locking unstable resonator excimer lasers", IEEE J. of Quantum Electronics, QE-19, pp1426-1436, 1983.

[19]. D.J.Bradley, "Methods of Generation ", Chapter 2 of "Ultrashort light pulses", S.L.Shapiro, ed., Springer-Verlag, 1977.

[20]. A. Yariv, "Optical Electronics", 3rd ed., Holt Rinehart and Winston, New York, 1985.

[21]. M.Born and E.Wolf ,"Principles of Optics", 5th ed., p396, Pergamon Press, Oxford, 1975.

[22]. J.J. Ewing and C.A.Brau " Laser action on the $^2\Sigma^+_{1/2} \rightarrow \, ^2\Sigma^+_{1/2}$ bands of KrF and XeCl", Applied Physics Letters, 27 pp350-352, 1975.

[23]. A.M.Hawryluk, J.A.Mangano, and J.H.Jacob, "Gain and absorption measurements in a KrF laser", Appl.Phys. Lett. 31, pp 164-166, 1977.

[24]. T.R.Loree, K.B.Butterfield, and D.L.Barker, "Spectral tuning of ArF and KrF discharge lasers", Appl.Phys.Lett. 32, pp 171-173, 1977.

[25]. H.F. Döbele, M.Höwekamp,"Tuning ranges of KrF and ArF excimer laser amplifiers and associated vacuum ultraviolet anti-Stokes Raman lines", Appl.Phys. B42, pp 67-42, 1987.

[26]. J.Goldhar and J.R.Murray, " Injection-locked, narrowband KrF discharge laser using an unstable resonator cacity", Optics

Letters, 1, pp 199-201, 1977.

[27]. R. Fedosejevs, X. X. Shan, and A. A. Offenberger, "Wavelength dependence of gain from 248.2 tO 248.4nm in a KrF discharge laser," J. Phys. D: Appl. Phys. 20, pp 912-916, 1987.

[28]. J. M. Halbout, S. Blit, W. Donaldson, and C. L. Tang, "Efficient phase-matched second-harmonic generation and sum-frequency mixing in Urea", IEEE J. of Quantum Electronics QE-15, pp 1176-1180, 1979.

[29]. J. Goldhar, W. R. Rapoport, and J. R. Murray, "An injection-locked resonator rare-gas halide discharge laser of narrow linewidth and high spatial quality" IEEE J. of Quantum Electronics, QE-16, pp 235-241, 1980.

[30]. G. G. Lombardi and J. M. Fukumoto, "Single-mode injection-seeded XeCl laser", Conference on Lasers and Electro-optics, Anaheim, April pp 25-29, 1988.

[31]. U. Ganiel, A. Hardy, and D. Treves, " Analysis of injection locking in pulsed dye laser systems", IEEE J. of Quantum Electronics, QE-12, pp 704-715, 1976.

[32]. Y. Zhu, R. A. Sauerbrey, F. K. Tittel, W. L. Wilson, Jr. and W. L. Nighan, "Injection controlled operation of a broadband excimer laser", A. I. P. coference proceedings 160, pp 30-32, 1987.

APPENDIX A

DESIGN OF THE BEAM TELESCOPE FOR THE ARGON ION LASER
AND DYE AMPLIFIER SYSTEM

In order to transport the output beam from the argon ion laser to the dye laser amplifier system a flexble beam telescope consisting of positive and negative focal length lenses was employed. As shown in Fig. A1, a negative focal length lens, F1, and positive focal lens, F2, are separated by a distance of S. The lenses are placed at a distance So from the source beam waist, ω_{01}, of the Argon ion laser and it is desired to form a new Gaussian beam waist, ω_{02}, at the position of the first dye laser amplifier cell. By varying the separation of the lenses, S, the position of the output of the beam waist can be varied. The distances are fixed by the geometric layout of the system at So = 2.2m and S1 = 1.5m. The focal lengths were chosen according to the available lenses as F1 = -0.1m and F2 = 0.25m.

The problem of finding the correct lens separation, S, to give the required beam waist position was solved using the ABCD law for Gaussian beams together with the ray matrices for the optical system [20].

For the optical ray matrix, M for the combined lenses and imaging distances we have

$$M = \begin{bmatrix} 1 & S_1 \\ 0 & 1 \end{bmatrix} \begin{bmatrix} 1 & 0 \\ -1/F_2 & 1 \end{bmatrix} \begin{bmatrix} 1 & S \\ 0 & 1 \end{bmatrix} \begin{bmatrix} 1 & 0 \\ -1/F_1 & 1 \end{bmatrix}$$
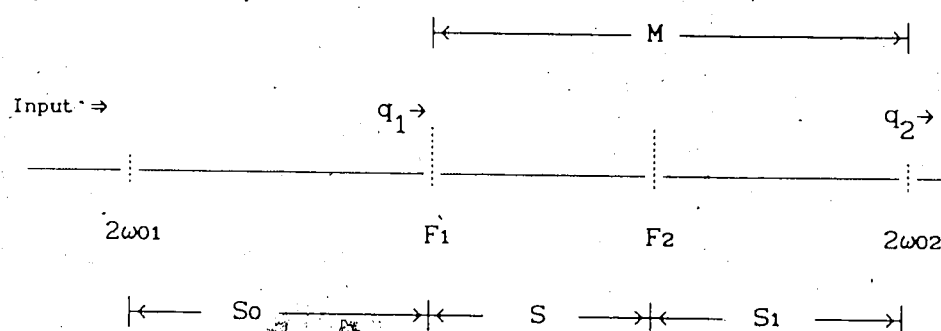
Fig.A.1 Beam telescope used to image the argon ion laser beam
waist into the first dye amplifier cell.

$$= \begin{bmatrix} (1-S/F_1) + S_1\{(-1/F_2)+[(-1/F_1)(1-S/F_2)]\} & S+S_1(1-S/F_2) \\ (-1/F_2) + [(-1/F_1)(1-S/F_2)] & 1-S/F_2 \end{bmatrix}$$

$$= \begin{bmatrix} A & B \\ C & D \end{bmatrix} \tag{A1.1}$$

For the Gaussian beam using the ABCD law, we obtain

$$q_1 = iZ_{01} + S_0$$

$$Z_{01} = \frac{\pi(\omega_{01})^2}{\lambda_0}$$

$$q_2 = iZ_{02} + Z$$

$$= \frac{Aq_1 + B}{Cq_1 + D} = \frac{A (iZ_{01} + S_0) + B}{C (iZ_{01} + S_0) + D}$$

$$= \frac{ACS_0 + BC - ACS_0 - AD}{-(CiZ_{01})^2 - (CS_0 + D)^2} iZ_{01} + \frac{-AC(Z_{01})^2 - AS_0(CS_0 + D) - B(CS_0 + D)}{- (CZ_{01})^2 - (CS_0 + D)^2}$$

$$= \frac{AD-BC}{(CZ_{01})^2 + (CS_0+D)^2} iZ_{01} + \frac{ACZ_{01}^2 + AS_0(CS_0+D) + B(CS_0+D)}{(CZ_{01})^2 + (CS_0 + D)^2} \tag{A1.2}$$

But we know that the determinants of the ray matrics used are all equal to 1.

$$\therefore \quad det \ |M| = 1$$

$$\therefore \quad AD - BC = 1$$

$$\tag{A 1.3}$$

Thus we obtain

$$q_2 = \frac{iZ_{01}}{(CZ_{01})^2 + (CS_0 + D)^2} + \frac{AC(Z_{01}^2 + S_0^2) + (AD + BC)S_0 + BD}{(CZ_{01})^2 + (CS_0 + D)^2}$$

$$= i\,Z_{02} + Z'$$

(A 1.4)

For q_2 to have its beam waist at the position S_1 requires that $Z' = 0$. Using the values : $S_0 = 2.2$ M, $f_2 = 0.25$ m, $S_1 = 1.5$ m, $f_1 = -0.1$ m, $\omega_{01} = 0.735 \times 10^{-3}$ m, and $\lambda_0 = 496.5 \times 10^{-9}$, the required lens separation is found numerically to be $S = 0.201$ m.

The resultant beam waist is then given by

$$\omega_{02} = \sqrt{\frac{\lambda_0\,Z_{02}}{\Pi}}$$

(A 1.5)

which gives a value of $\omega_{02} = 89 \mu m$ at the entrance of the first dye cell.